MNRAS 000, 1–17 (2020) Preprint 31 July 2021 Compiled using MNRAS LATEX style file v3.0

Variable White Dwarfs from Gaia DR2/EDR3 vetted by ZTF

Thinh Nguyen,[1]★ Laurent Eyer,[2]† Lorenzo Rimoldini,[3] Ashish Mahabal,[4] Marc Audard,[2] Pedro García-Lario,[5] Panagiotis Gavras,[6] Krzysztof Nienartowicz[3,7]

[1]*Department of Astrophysics and Planetary Sciences, Villanova University, 800 E. Lancaster Avenue, Villanova, PA, 19085, USA*
[2]*Department of Astronomy, University of Geneva, Chemin Pegasi 51, 1290 Versoix, Switzerland*
[3]*Department of Astronomy, University of Geneva, Chemin d'Ecogia 16, 1290 Versoix, Switzerland*
[4]*Division of Physics, Mathematics, and Astronomy, California Institute of Technology, Pasadena, CA 91125, USA*
[5]*European Space Astronomy Centre (ESA/ESAC), Villanueva de la Canada, 28692 Madrid, Spain*
[6]*RHEA for European Space Agency (ESA), Camino bajo del Castillo, s/n, Urbanizacion Villafranca del Castillo, Villanueva de la 21 Cañada, 28692 Madrid, Spain*
[7]*Sednai Sarl, Rue des Marbriers 4, 1204 Geneva, Switzerland*

Accepted XXX. Received YYY; in original form ZZZ

ABSTRACT

The publications of *Gaia* DR2 and EDR3 have brought major improvements on stellar photometry and astrometry, particularly regarding the impressive description of white dwarf sequences. Following previous results on the detection of variable white dwarfs by *Gaia* DR2, this study aims to refine the list of candidates with the new measurements and analyze the physical origins of white dwarf variability. As a result, we obtain distinguishable regions of various types of variable white dwarfs such as ZZ Ceti, V777 Herculis, GW Virginis, and DQV stars. We present 343 ZZ Ceti candidates and 43 variable white dwarf-main sequence binaries, while estimate that there are 99 V777 Herculis, 102 GW Virginis, and 47 DQV candidates. In addition, for all sets of candidates but ZZ Ceti, Zwicky Transient Facility (ZTF) DR5 time series are examined through Lomb-Scargle analysis and Chi-square test to verify the stars' periodicity and variability. For the periodic variable stars, the periods range from 6.5 minutes to 2 days and the amplitudes range from 0.06 to 0.4 mags. This list of variable white dwarfs from *Gaia* EDR3 is one of the largest samples so far, potentially multiplying the number of known variable white dwarfs by several times. Moreover, there are 16 variable white dwarf candidates whose *Gaia* time series are available. Comparison with ZTF data for these stars shows that 33% of the sample result in similar periods while being studied by two independent surveys. Thus, the result emphasizes the potential of *Gaia* and ZTF in detecting variable white dwarfs.

Key words: white dwarfs – stars: oscillations – binaries: general

1 INTRODUCTION

We are in an epoch of large data growth in optical astronomy. There is a challenge not only in the growth of mere data volume but also in the variety of survey properties and data types. Among all the surveys, the *Gaia* mission (Gaia Collaboration et al. 2016a), a cornerstone mission of the ESA science program launched at the end of 2013, is an unprecedented mission. On a single space platform, there are repeated astrometric, photometric, spectrophotometric, and spectroscopic measurements over the entire celestial sphere.

The *Gaia* DPAC consortium (Mignard et al. 2008) has taken care of the data reduction, calibration, and analysis of the *Gaia* data as well as has prepared the data products to be published by ESA in a stepwise manner. The goal of this approach is to improve the data reduction, to lower random and systematic errors in all of the data products, and to gradually increase the number of published sources and data products.

The same iterative approach was followed for publishing the *Gaia* photometric time series. For the first *Gaia* Data Release (September 2016; Gaia Collaboration et al. 2016b), a selection of 3,194 variable stars near the South Ecliptic pole, which covered partially the Large Magellanic Cloud, was published with their G-band time series. For the second *Gaia* Data Release (April 2018; Gaia Collaboration et al. 2018a), more than half a million variables objects were published with their G, integrated BP, and RP time series. By *Gaia* standards, even if half a million variable objects represented a relatively small fraction of the entire data set, these variable star samples were already among the largest published catalogues for some variability types (e.g. RR Lyrae stars, large-amplitude long-period variable stars, δ Scuti stars).

Along with the *Gaia* DR2, a performance verification paper was published by Gaia Collaboration et al. (2019) to describe the variability across the observational Hertzsprung-Russell (HR) Diagram, which included distinctive variability features for the white dwarf sequence. The locations of some variable white dwarfs known from the literature were expectedly in very precise locations and sometimes in surprising locations. For example, the cataclysmic variables from

★ E-mail: tnguye55@villanova.edu
† E-mail: Laurent.Eyer@unige.ch

the literature seemed to have a clump where some pulsating white dwarfs are anticipated (see fig. 7 of Gaia Collaboration et al. 2019).

In this study, we focus on variable white dwarfs. The white dwarfs are classified according to the spectra from their atmosphere. The main types are DA (hydrogen dominated), DB (helium dominated), DAB (hydrogen and neutral helium), DO (hydrogen and single ionized helium), DQ (carbon dominated), DZ (metal rich), DC (featureless continuum). When these white dwarfs are variable, the suffix V is concatenated to the spectral type. The classical DAVs are ZZ Ceti stars, DBVs are V777 Herculis stars, and DOVs are GW Virginis stars (also called PG 1159 stars). All these stars are pulsating in non-radial gravity modes, due to the κ-mechanism related to the composition of their thin envelope (Winget & Kepler 2008). It can be remarked that these pulsating stars are among the first objects for which asteroseismic studies could be performed to unveil some of their physical properties (Winget et al. 1991). On the other hand, unlike DAV, DBV, and DOV stars, the source of DQV's variability is suggested not to come from pulsation. Particularly, the high magnetic activities of DQV stars can hinder the pulsation mechanism (Tremblay et al. 2015), and DQV stars only have a single oscillation mode while other pulsating white dwarf types usually have multiple independent modes (Williams et al. 2016). Thus, it is currently believed that the mechanism of DQV's variability is rotation with magnetic cool spots (Williams et al. 2016; Macfarlane et al. 2017). Furthermore, there are also other possible physical origins of white dwarf variability (Percy 2011). For instance, a white dwarf can be in an accreting system and can show up as a cataclysmic variable. Also, white dwarfs can have spots (Brinkworth et al. 2005) as already mentioned or can be in a binary system that is eclipsing or presenting ellipsoidal variations.

Within *Gaia* data, the published averaged statistics can help to infer the variability of stars whose time series have not been released (see for example Belokurov et al. 2017; Mowlavi et al. 2021; Guidry et al. 2021). Using the relationship between the uncertainty of the mean flux and its standard deviation, corrected for an estimation of the instrumental and photon noises (Eyer 1998), Eyer et al. (2020) explored the variability of the white dwarfs identified by Gentile Fusillo et al. (2019). The growth in the number of known and proposed objects is quite impressive. Specifically, the number of ZZ Ceti stars in the compilation of pulsating white dwarfs published by Córsico et al. (2019) is 261, while in the list of Eyer et al. (2020) the number is is 373. As for the V777 Herculis stars, the numbers are 27 and 345, respectively. For GW Virginis stars, there are 21 objects (Althaus et al. 2010) versus 783. This growth is surprising, although we know that any problems in the *Gaia* calibration and outlying values would produce false detections and that the list of Eyer et al. (2020) includes candidates. Moreover, any other variability-inducing phenomena such as binarity or spots would lead to erroneous classifications. Therefore, the goal of this article is to verify the reliability of the list of 5837 variable white dwarfs proposed by Eyer et al. (2020) using *Gaia* EDR3 (Gaia Collaboration et al. 2021; Riello et al. 2020) and the Zwicky Transient Facility (ZTF) DR5 surveys (Bellm et al. 2019) as well as to compare the candidates with the literature. We aim to update Eyer et al. (2020)'s list of white dwarf candidates with adjusted criteria employing *Gaia* EDR3 measurements while also considering other variable types. In addition, we examine stars that have time series in the *Gaia* DR2 archive (Holl et al. 2018) and check the photometry of ZTF to compare the consistency between the two surveys.

The article is structured as follows. Firstly, we present some general properties of the *Gaia* and ZTF surveys in Section 2. In Section 3, we describe how the ZTF time series are cleaned and the method to search for periods. We show the criteria that are used to select and refine eligible candidates from *Gaia* EDR3 in Section 4. Section 5 discusses the effectiveness of our methods by applying them to a list of known pulsating white dwarfs. The subsets of ZZ Ceti, V777 Herculis, GW Virginis, and DQV are commented, analyzed, and compared with the literature in Sections 6, 7, 8, and 9, respectively. In Section 10, we compare published *Gaia* time series with those of ZTF. Observations on the amplitude of some of these time series help us introduce a criterion to select white dwarf-main sequence binary systems, which is discussed in Section 11. Section 12 presents the cross-match of our catalogue with known cataclysmic variables and known white dwarf-main sequence binaries. Finally, in Section 13, we discuss further implications of the study and provide conclusions based on our analysis.

2 DATA

The data for this study are obtained from the public archives of *Gaia* DR2, *Gaia* EDR3[1], and ZTF DR5[2]. For *Gaia*, we utilize both the survey's DR2 and EDR3 data, specifically the mean photometry (Evans et al. 2018; Riello et al. 2020) and astrometry (Lindegren et al. 2018, 2020), to determine the target locations in the observational Hertzsprung-Russell Diagram. As EDR3 improves in accuracy with respect to DR2, we use the most recent data archive to refine the results found in Eyer et al. (2020) and conduct further study. On the other hand, because EDR3 does not include time series data, we employ DR2's published time series in the *G*, *BP*, and *RP* bands (Holl et al. 2018) for analyzing variability. For ZTF DR5, we study its time series in both *g* and *r* bands.

In the following paragraphs, we examine some general properties of *Gaia* and ZTF photometric time series. From the *Gaia* DR2 catalogue of white dwarfs (Gentile Fusillo et al. 2019), about 2000 white dwarfs candidates are chosen randomly over a wide range of magnitudes. For each star, the number of observations is recorded from the ZTF time series. According to Figure 1, *Gaia* sources have fewer number of field of view transit observations than those of ZTF and the majority of stars from *Gaia* have around 40 to 50 measurements. On the other hand, ZTF sources, particularly in the *r* band, have the highest number of observations per star. In some cases, ZTF DR5's number of observations exceed 500 measurements per star.

Regarding the photometric precision diagram in Figure 2, another random sample from Gentile Fusillo et al. (2019)'s catalogue is obtained. Among them, 1490 stars have ZTF DR5 time series in both bands with at least 2 measurements per time series. The standard deviation of the time series (σ_G) and the standard deviation of the mean magnitude ($\sigma_{\bar{G}}$) of *Gaia* data are estimated using the number of per CCD observations (`phot_g_n_obs`) and the photometric mean flux over its error (`phot_g_mean_flux_over_error`):

$$\sigma_G = \frac{1.086\sqrt{\texttt{phot\_g\_n\_obs}}}{\texttt{phot\_g\_mean\_flux\_over\_error}}. \quad (1)$$

$$\sigma_{\bar{G}} = \frac{1.086}{\texttt{phot\_g\_mean\_flux\_over\_error}}. \quad (2)$$

The coefficient 1.086 is an approximation of $\frac{2.5}{ln(10)}$, which is obtained when calculating the propagation of error from a flux-magnitude relationship. In Figure 2, the x-axis illustrates the mean magnitude and

[1] https://gea.esac.esa.int/archive/
[2] https://irsa.ipac.caltech.edu/Missions/ztf.html

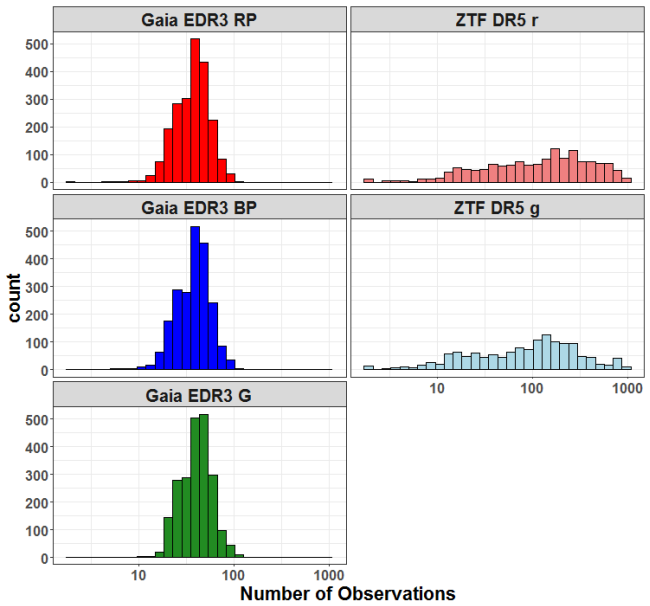

Figure 1. The histograms show the number of observations in each band for each survey. We randomly choose around 2000 white dwarf candidates over a wide range of magnitude to measure their number of measurements. ZTF has on average more number of observations per star than the number of Field-of-View transits per star of *Gaia*.

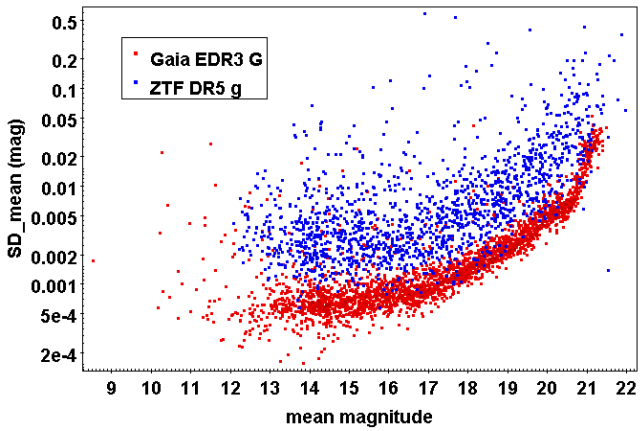

Figure 2. We compare the standard deviation of the mean magnitude (Equation 2) as a function of the mean magnitude of *Gaia* EDR3 and ZTF DR5 times series for individual sources. Around 2500 white dwarf candidates are chosen randomly over a wide range of magnitude to measure their standard deviation. The diagram illustrates that *Gaia* reaches higher precision than ZTF, but ZTF's envelope is close enough to *Gaia*'s that we can use ZTF time series to study *Gaia* candidates.

the y-axis shows the standard deviation of mean magnitude (Equation 2). For ZTF, $\sigma_{\bar{g}}$ is calculated by dividing the time series's standard deviation by the square root of the number of measurements. The figure demonstrates that *Gaia* has more precise individual photometric measurement than ZTF. However, the ZTF's distribution is close enough to that of *Gaia* that ZTF data can be reliably used to analyze *Gaia*'s variable white dwarf candidates even when photometric time series are not available in *Gaia*.

There are also differences between the two surveys in terms of the time covered and time sampling. The time covered by these surveys is from July 2014 to June 2016 for *Gaia* DR2 and from March 2018

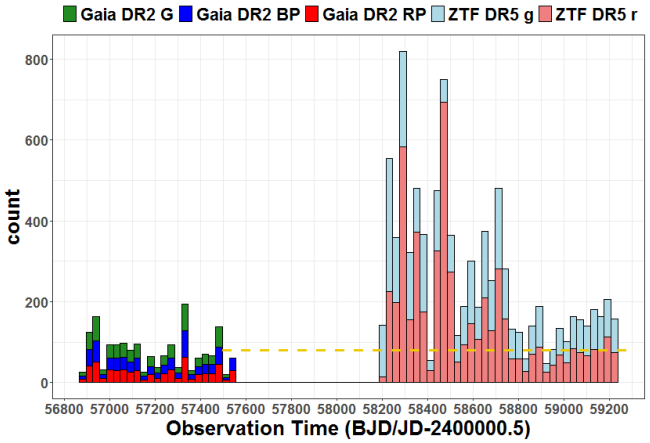

Figure 3. Histograms show the distribution of observations in time. The data used to make this histogram comes from the candidates whose time series data is available in *Gaia* DR2 (referred in Section 10). As shown in the diagram, ZTF's time coverage is not far from that of *Gaia*. Thus, it is reasonable to use ZTF time series to verify the *Gaia* variable white dwarf candidates. The dashed line indicates the future *Gaia* data releases. More data will also be available for ZTF.

to February 2021 for ZTF DR5. The time range of data collection for each survey is shown in Figure 3. For *Gaia*, the distribution of measurements in time is presented for candidates whose time series are published. It should be pointed out that *Gaia* uses barycentric julian date (BJD) while ZTF uses julian date (JD), however, the difference between the two units is not significant for the purpose of this plot. Since the time gap between *Gaia* DR2 and ZTF DR5 is only around 2 years, we can use ZTF's time series as a comparison with *Gaia*. When *Gaia* publishes more time series in the upcoming data releases, that time gap will disappear.

Moreover, ground-based surveys like ZTF typically have a spectral window with peaks around multiples of 1 cycle per day. In the case of *Gaia*, the period of rotation is 6 hours, so the peaks are at multiples of 4 cycles per day. Thus, the combination of the surveys with different observing strategies can lift aliasing ambiguities.

3 CLEANING ALGORITHM AND ANALYSIS METHOD

We use all data points in the *Gaia* time series for the analysis. On the other hand, initial looks on the ZTF time series show that they often contain contaminating measurements. Thus, we need to remove those outliers before using the data. The ZTF light curves are cleaned by setting limits for magnitude and selecting convenient time intervals. The outliers by magnitude are determined as follows. The standard deviation is estimated from the IQR value of the time series. Data points that are beyond 3 times the standard deviation around the median will be removed. On average, around 4.1% of the ZTF time series measurements are removed as magnitude outliers by using our algorithm. For our time interval selection, if two successive data points are separated by more than 150 days, we preserve the side with more data points for analysis. This selection ensures the homogeneity and the good density of data points in the cleaned time series.

We acknowledge that there is another cleaning method which removes contaminating measurements by restricting the parameters within ZTF time series, such as *catflag*, *sharp*, and *limitmag* (Guidry et al. 2021). Compared to our method described above, these criteria are better in terms of yielding a larger significance of the retrieved

periods. However, the periods remain similar and some of the light curves are removed completely by Guidry's criteria, even though these light curves are proved to be periodic from our method. Thus, we maintain our cleaning method to remove outliers from ZTF measurements.

The cleaned time series are analyzed through the Lomb-Scargle analysis to obtain the peak frequency of variability (Lomb 1976; Scargle 1982). Specifically, the *lsp* function in *R* (Ruf 1999) is used to conduct the analysis and compute the normalized power spectrum. Parameters utilised in the function are scanned frequency from 0 to 400 cycles per day, *ofac* (oversampling factor) of 8, and *alpha* (significance level) of 0.01. After obtaining the peak frequency, the corresponding period is computed, and thus the phase of each measurement can be determined from that period. With the phase data, we plot the folded light curve for each star. The imagery version of the reduction steps is displayed in Figure 4.

With the calculated frequencies from Lomb-Scargle, the preliminary test to verify the variability behavior of a star is to compare the frequencies recovered in the ZTF g and r bands. If the two frequencies are similar, the stellar variations are likely periodic. However, there are exceptions. If the two frequencies are exactly one day or multiples of one day, the light curves are affected by aliasing effect and thus cannot be used to obtain the correct frequencies. In the Lomb-Scargle period search, the full width at half maximum of the peak is the uncertainty of the frequency. By examining various values of the two parameters, it is empirically found that the line width is inversely proportional to α times the time range (Cuypers 2012). Therefore, for the g and r frequency to be similar, their difference must lie within the largest line width. Thus, the smaller time range between g and r band data will be selected for the comparison equation. The mathematical definition for "similar frequency" is expressed as follows:

$$|\text{frequency}_g - \text{frequency}_r| < \frac{\alpha}{\min(t_{\max} - t_{\min})}, \tag{3}$$

in which α is typically equal to 0.7.

While the Lomb-Scargle periodogram technique is used to detect the periodic variability of the star, it can be inaccurate if the star does not have a stable period. Thus, we also employ the Chi-square test as an additional method to validate the star's variability. The examined null hypothesis is that the star has constant magnitude over time, and thus its Chi-square value is calculated using Equation 4,

$$\chi^2 = \sum_i \frac{(m_i - \bar{m})^2}{\sigma_i^2}, \tag{4}$$

where m_i is the measured magnitude, $\bar{m}$ is the weighted mean of the time series using σ_i^{-2} as weights, and σ_i is the uncertainty of each measurement. Combined with the degrees of freedom, this Chi-square value is converted to the p-value for each star by using the `pchisq` function in R (Becker et al. 1988) to establish a common comparable standard. The significance level for this study is calibrated with non-variable stars defined as follows. One hundred white dwarfs from Gentile Fusillo et al. (2019) that are outside the instability strips of any defined pulsating white dwarf and have standard deviation lower than a certain threshold (will be defined in Section 4) are selected for the calibration. For each star, we calculate the p-value of its ZTF time series. We set the probability for type I error to be 6%, meaning at most 6 stars in our 100-star sample are misclassified as variable stars. This correspond to the p-value limit of 1.49e-05 for ZTF g band and 4.87e-05 for ZTF r band. In other words, if the p-value is larger than the limit, the null hypothesis cannot be rejected and the star is non-variable. On the other hand, if the p-value

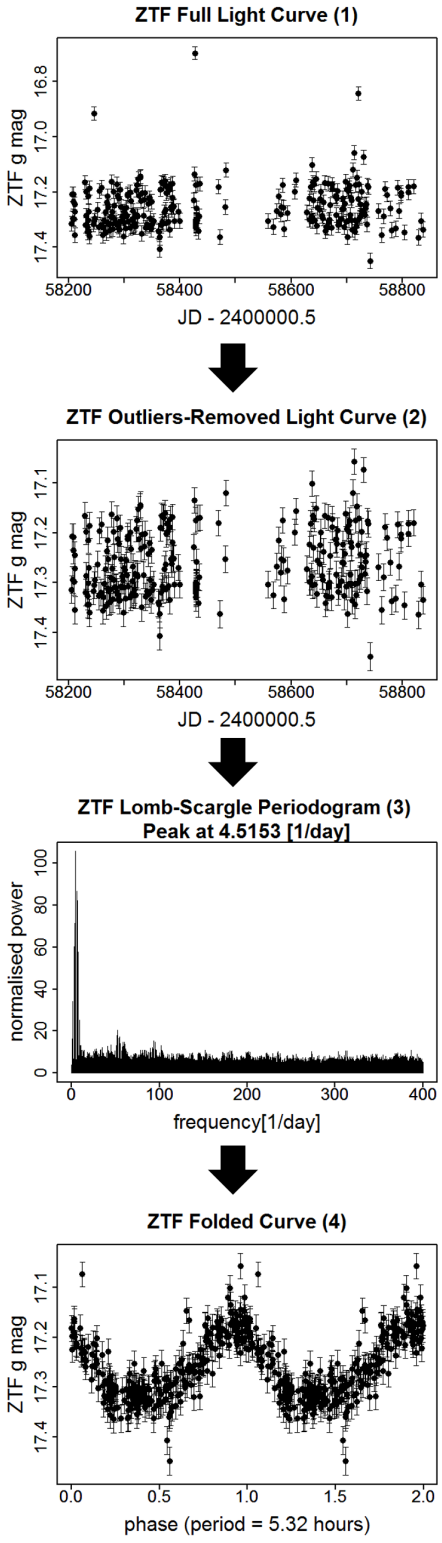

Figure 4. The diagram shows the steps to reduce the raw ZTF DR5 light curve of the candidate Gaia DR2 2061416695278519808 into folded light curve. From Step (1) to (2), outliers are removed from the raw data based on their times and magnitudes. For this target, there were initially 279 measurements and 3 of them were removed as outliers. The output is examined by Lomb-Scargle analysis to return the peak frequency of variability at the maximum power, which is displayed in Step 3. In Step 4, the period calculated from the peak frequency is used to create a folded light curve.

is smaller than the limit, the star is variable. Furthermore, we define that a star is declared as variable when at least one of two bands demonstrates non-constancy according to the Chi-square test.

It should be noted that we assume the uncertainties from ZTF measurements to be consistent. Also, in many cases, the amplitude of the pulsating white dwarfs is smaller than the uncertainty of ZTF measurements. For example, the peak-to-peak amplitude of GW Vir candidates is from 0.01 to 0.15 mags (Althaus et al. 2010), while the typical ZTF standard deviation (Figure 2) is from 0.005 to 0.1 mags. Therefore, the classification from Chi-square may not precisely determine the variability of every star in the subsets.

4 VERIFICATION OF VARIABLE WHITE DWARF GROUPS WITH *GAIA* EDR3

With regard to the publication of *Gaia* EDR3, the initial step of the study is to evaluate 5837 variable white dwarf candidates in Eyer et al. (2020) with the new measurements. As it is not guaranteed that one star has a similar source identifier across different data releases, we performed a conversion from the *Gaia* DR2 source IDs provided in Eyer et al. (2020)'s list to the new EDR3 IDs by using `gaiaedr3.dr2_neighbourhood` data in EDR3 data archive (Gaia Collaboration et al. 2021). As a result, 5837 targets in the DR2 list result in 6454 corresponding stars in EDR3. We apply the preliminary cut as shown in equations 2–5 of Gentile Fusillo et al. (2019) to remove those contaminating targets that are outside the viable white dwarf region. As a result, 5032 stars are located at the white dwarf sequence on the HR diagram.

The locations of these 5032 stars are displayed in the sky plot on the left-hand side of Figure 5. As we expect the targets to be evenly distributed across the sky, it is very peculiar that patterns such as over-density regions and defined curves appear in the sky plot. Thus, we refine our selection by utilising restrictions on photometric and astrometric parameters. Also, we did not introduce an additional restriction on the parallax in respect to the one in Gentile Fusillo et al. (2019), which limits the `parallax_over_error` to be larger than 10. Figure 5 displays the resultant sky plot (right) after the criteria are applied. All the clumped regions are removed and the plot shows the expected uniformity. The criteria are listed below:

$$\begin{aligned}&\texttt{astrometric\_excess\_noise} <= 1\,\texttt{mas}\\&\texttt{phot\_g\_mean\_mag} <= 19.5\,\texttt{mag}\\&\texttt{visibility\_periods\_used} >= 9\\&\texttt{ruwe} <= 1.6.\end{aligned} \tag{5}$$

As a result, only 3586 out of 5032 candidates (71%) of EDR3 targets are eligible for the study.

After cleaning the data set, we proceed to determine the variability of the stars. Figure 6 displays the G-band estimated standard deviation of the per CCD time series (calculated in Equation 1) as a function of G magnitude. Compared to figure 2 of Eyer et al. 2020, the constant noise level has a different shape in EDR3 from DR2's photometry. Thus, we apply a new criterion for detecting variability with respect to the new measurements. We propose

$$\begin{aligned}\text{threshold} = {} & 0.0274482\,\texttt{phot\_g\_mean\_mag}^2\\&- 0.800421\,\texttt{phot\_g\_mean\_mag}\\&+ 3.9427 + \log_{10}(1.12)\end{aligned} \tag{6}$$

as an updated threshold, which is presented by the blue line in Figure 6, to select variable stars according to EDR3. We determine the blue curve by fitting the reduction in density of standard deviation of per CCD time series measurements versus G between the assumed variable and non-variable stars. The variable white dwarf candidates are red coded in Figure 6 and amount to 1743 objects in our selection. Figure 7 shows the location of our variable candidates on the colour-absolute magnitude diagram, in which there are noticeable clumps along the white dwarf sequence. The ZZ Ceti clump is the densest region. In the bluer and brighter region of the plot, two broad over-densities are noticeable, which are likely associated with the V777 Herculis stars and the GW Virginis stars. Right below the V777 Herculis region, there is a clumped region that could host DQ variables. Furthermore, above the white dwarf sequence, a dense group ranging from -0.5 to 0.3 colour index is noticeable. We suspect that this group hosts binary systems, which we will discuss in detail in a later section. Due to the visual and illustrative purpose, Figures 7, 8, 9, and 17 are limited to a colour range from -0.8 to 0.8 mag. This removes three targets that are redder than than 0.8 mag: Gaia EDR3 661504265860547200, Gaia EDR3 4652123895783242112, and Gaia EDR3 1534384148897669248. From our classifications later in this section, they include a high-amplitude candidate and two low-amplitude candidates, accordingly.

After determining the potential variable stars, we investigate their cause of variability, particularly pulsation or binarity. To determine the pulsation behavior of a star, we utilize the intrinsic amplitude proxy, which can be computed with respect to the proposed noise threshold as:

$$\begin{aligned}&\text{log\_intrinsic\_ampl\_proxy\_g} =\\&\log_{10}\sqrt{\sigma_G^2 - 10^{\text{threshold}-\log_{10}(1.12)}} < -1.15.\end{aligned} \tag{7}$$

In Equation 7, we lower the threshold by the value of $\log_{10}(1.12)$. This corresponds to the noise level, which passes in the middle of the distribution of the objects identified as non-variable in Figure 6.

The intrinsic amplitude proxy is colour-coded within the colour-absolute magnitude diagram shown in Figure 8. Moreover, after empirically examining different values and comparing with figure 2 of Eyer et al. (2020), variable white dwarfs that gather at known pulsating instability strips generally have the log of intrinsic amplitude proxy in G band smaller than -1.15 (0.07 mag). Given our selection of objects, variable stars from Figure 6 that have intrinsic amplitude proxy lower than 0.07 mag have a high possibility to be pulsating. Thus, in our Figure 8, we only choose the candidates within this limit, which are referred to as low-amplitude candidates, to simplify the diagram and to better address the pulsating groups. There are 1560 low-amplitude candidates and 183 high-amplitude candidates. In Figure 8, over-density regions of known pulsating white dwarf types, namely ZZ Ceti stars (BP−RP ranges from 0 to 0.1 and absolute G magnitude is around 12 mag), V777 Herculis stars (BP−RP ranges from -0.35 to -0.15 and absolute G magnitude ranges from 9.8 to 11.2 mag), and GW Virginis stars (BP−RP ranges from -0.6 to -0.4 and absolute G magnitude ranges from 7 to 10 mag), appear clearly. We also notice two crowded regions: one in the blue side of the V777 Herculis stars (from absolute G magnitude 11 to 13 and from BP−RP colour index -0.5 to -0.2) and one with the colour index ranging from 0.3 to 0.5. The former group might include warm DQV stars, while the latter group might consist of the rarer DQV stars. Regarding the stars that have a high amplitude (intrinsic amplitude larger than 0.07 mag), we suspect that they are binary systems. These stars form two over-density regions: one on the right of GW Virginis's instability strip and one next to the ZZ Ceti's instability strip.

As shown in Figure 8 and also in figure 2 of Eyer et al. (2020), ZZ Ceti stars' over-density in the observational HR diagram has an elliptical shape, while those of V777 Herculis and GW Virginis stars

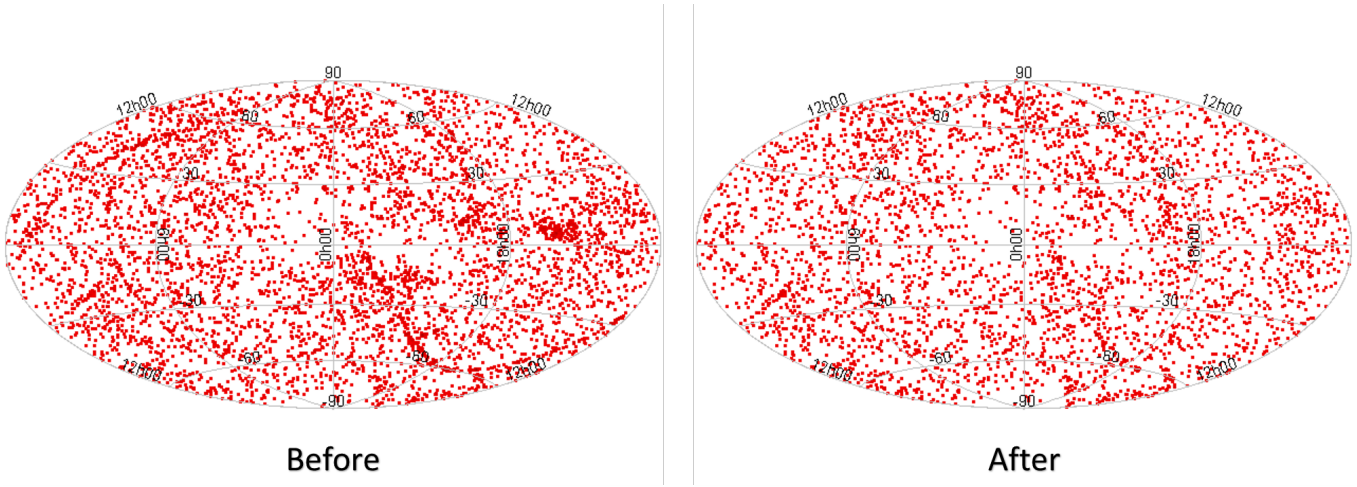

Figure 5. The criteria on the accuracy of measurement are applied to the EDR3 measurement to remove the over-density regions as well as peculiar aligned patterns in the original sky plot (left) in Galactic coordinates. After the selection, the resultant sky plot (right) has a relatively uniform distribution of stars with some minor over-densities. The accuracy criteria reduce the number of candidates from 5032 to 3586.

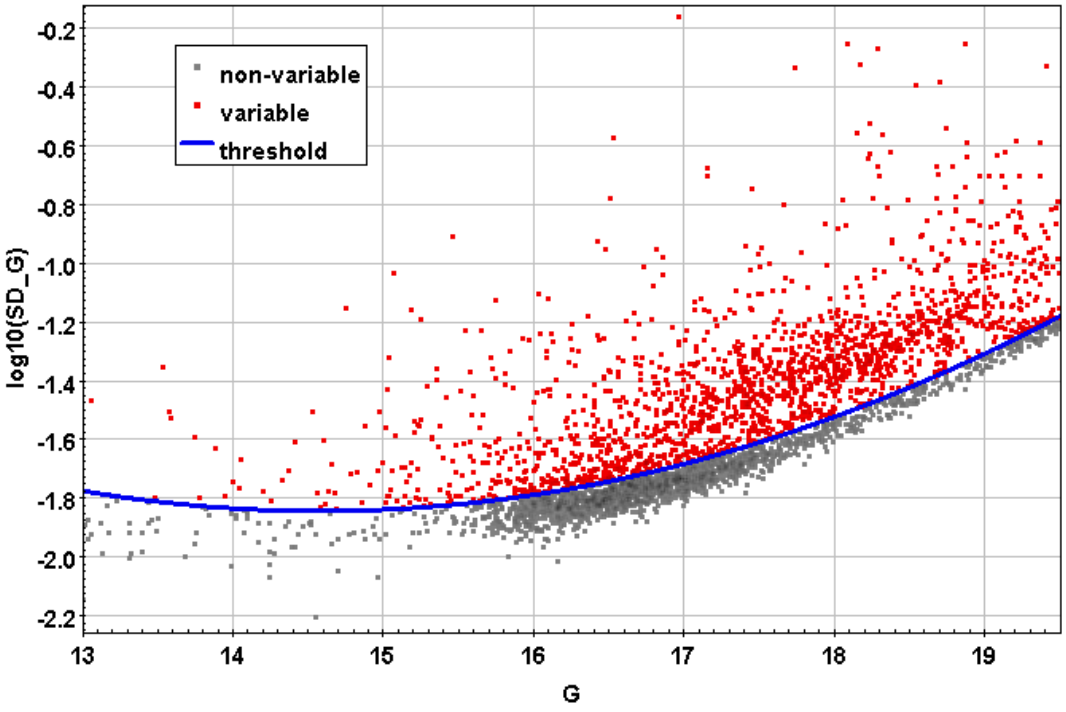

Figure 6. The estimated standard deviation of the *G*-band per CCD time series (Equation 1) is plotted as a function of mean *G* magnitude to better select *Gaia* DR2 variable white dwarf candidates with photometric data from *Gaia* EDR3. All candidates in this figure are refined by applying restrictions on the measurement's accuracy. An updated noise threshold (Equation 6) was computed to fit the new photometric measurements. In this selection, among 3586 targets with reliable measurements, 1743 white dwarfs with the red colour-code are expected to be variable according to *Gaia* EDR3 data.

appear as long strips. Thus, we use ellipses to generalize the shape of the variability regions and to select variable white dwarf candidates. The shape of the ellipses is adjusted to match with the border of the clumped areas. The ellipses corresponding to the variability regions of ZZ Ceti stars, V777 Herculis stars, GW Virginis stars, and DQV stars are described by Equations 8, 9, 10, and 11, respectively:

$$\sqrt{\left(\frac{x-0.038}{0.048}\right)^2+\left(\frac{y-11.85}{0.17}\right)^2}=1 \tag{8}$$

$$\sqrt{(x+0.37)^2+(y-10.1)^2}+\sqrt{(x+0.16)^2+(y-11.25)^2}=1.177 \tag{9}$$

$$\sqrt{(x+0.4)^2+(y-10)^2}+\sqrt{(x+0.59)^2+(y-7)^2}=3.007 \tag{10}$$

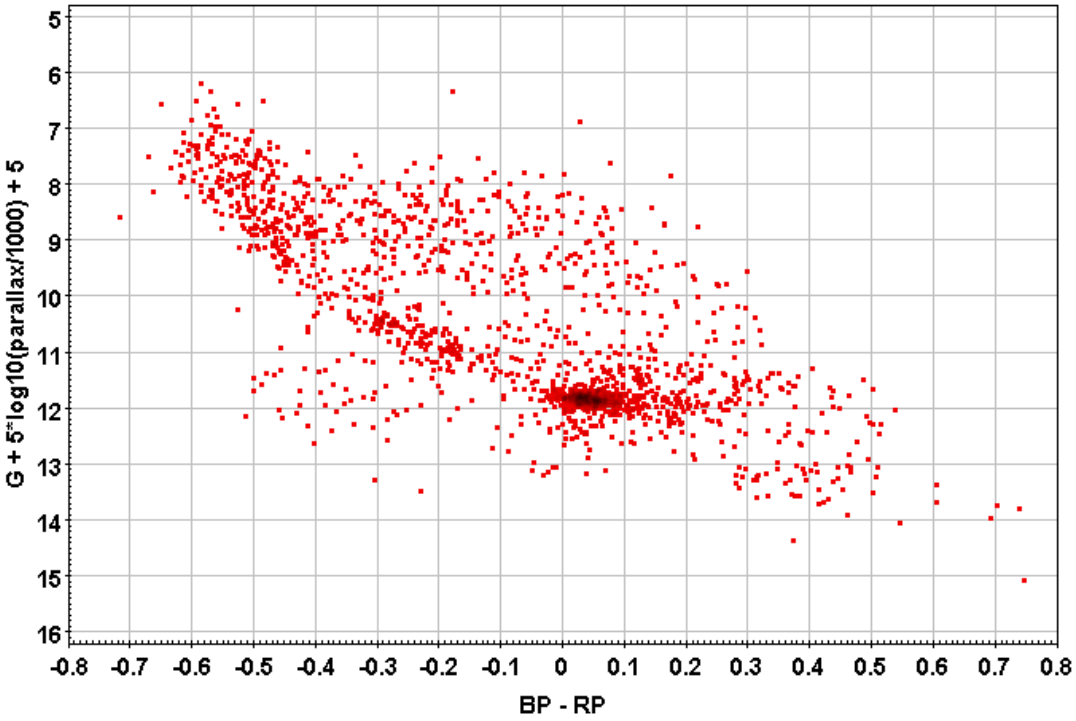

Figure 7. The colour-absolute magnitude diagram of the new selection from Figure 6. *G*, *BP*, and *RP* are the *Gaia* mean magnitudes of the corresponding bands. We distinguish several regions of interest along the white dwarf sequence such as the clumps of pulsating white dwarfs, binaries, and DQV stars. It should be noted that for better visualization of most of the targets, three of them (redder than 0.8 mag) were excluded.

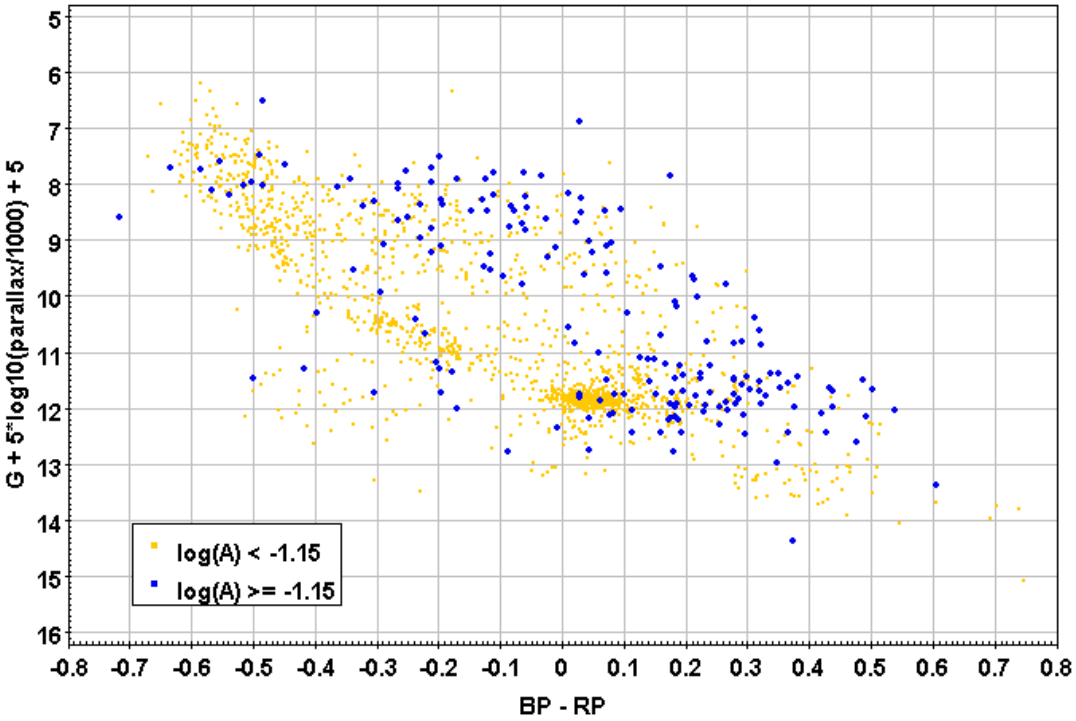

Figure 8. The colour-absolute magnitude diagram of variable white dwarfs in Figure 7 is shown with an amplitude criterion. Stars with intrinsic amplitude A in the G band smaller than 0.07 mag ($\log A < -1.15$) have a high chance to be pulsating. The result yields consistency as clumped regions of known variable white dwarf types such as ZZ Ceti, V777 Herculis, GW Virginis, and DQV are noticeable in the diagram. Also, stars that have a high intrinsic amplitude (larger than 0.07 mag) are suspected to be binary systems. According to this classification, there are 183 high-amplitude candidates and 1560 low-amplitude candidates.

$$\sqrt{(x+0.5)^2+(y-10)^2}+\sqrt{(x+0.24)^2+(y-14)^2}=4.024, \quad (11)$$

where x denotes `phot_bp_mean_mag - phot_rp_mean_mag` and y denotes `phot_g_mean_mag + 5*log10(parallax/1000) + 5`. Any stars that are inside the ellipse are considered as candidates of the corresponding variable type. Furthermore, we limit our candidate selection to stars whose log of intrinsic amplitude proxy is smaller than -1.15, as we discussed before that this suggests pulsating variables. The above defined ellipses identify 343 stars as ZZ Ceti candidates, 103 stars as V777 Herculis candidates, 132 stars as GW Virginis candidates, and 49 stars as DQV candidates. Figure 9 displays the variable white dwarf candidates selected within these ellipses on the colour-magnitude diagram.

Figure 10 displays the histograms of the intrinsic amplitude proxy for our 4 groups of variable white dwarf candidates. The distributions are normalized by their area. According to Althaus et al. (2010), ZZ Ceti and V777 Herculis stars have higher pulsating amplitude than GW Virginis and DQV stars. In our diagram, the ZZ Ceti type has a peak at around 0.04 mag, which is the largest intrinsic amplitude proxy among our subsets. However, while Althaus et al. (2010) states that V777 Herculis stars have a much higher and broader range of amplitude than GW Virginis and DQV stars, our results indicate the opposite. In Figure 10, the amplitude of V777 Herculis stars has a peak at 0.006 mag and ranges from 0.002 mag to around 0.05 mag. GW Virginis stars have a more uniform intrinsic amplitude proxy distribution with a peak at 0.007 mag when ranging from 0.002 mag to about 0.07 mag. Besides, DQV stars have a rather flat amplitude distribution (from 0.004 to more than 0.07 mag) with a larger average amplitude than that of V777 Herculis and GW Virginis.

5 EFFECTIVENESS OF LOMB-SCARGLE AND CHI-SQUARE METHODS TO DETECT WHITE DWARF VARIABILITY

Before applying the Lomb-Scargle analysis and Chi-square test to our candidates, we will validate their effectiveness in examining stellar variability by applying the methods to known pulsating white dwarfs. Among all types of pulsating white dwarfs, we choose GW Virginis stars for the test as they have brighter magnitudes (i.e., higher signal-to-noise ratio). A list of all known GW Virginis stars in literature is obtained from table 5 of Althaus et al. (2010). Among the 21 known GW Virginis stars, 16 have ZTF DR5 time series.

According to Table 1, the Chi-square test confirms that 14 of the 16 stars (87.5%) are variable either in the g or r bands. Even though the Chi-Square test provides a good indication on whether a star is variable, it might not be always effective in determining variability because pulsating white dwarfs often have small amplitudes. Thus, we should use the test as a suggestion rather than a definite claim. We also conducted a Lomb-Scargle analysis with scanned frequencies ranging from 0 to 400 cycles per day (3.6 minutes), which covers the known range of GW Virginis stars' frequency. However, a period similar to the one from the literature with a significant peak in the Lomb-Scargle spectrum was recovered only for the star PG 1707+427 (*Gaia* source ID 1355161726346266112). For the rest of the targets, the recovered periods were either not consistent with the values provided by previous studies or not correspondent to a significant peak in the spectrum. Moreover, as remarked by Guidry et al. (2021), comparisons between high-speed photometry and ZTF show that ZTF time series are not always sufficient for Lomb-Scargle to detect the correct pulsation period in some stars, particularly for cases with high-frequency pulsation or complex pulsation modes. Therefore, the Lomb-Scargle analysis may not effective in detecting pulsating white dwarf's periods given the time sampling of ZTF. On the other hand, Lomb-Scargle analysis can still be useful for variability of other nature such as binarity, which is explored in the later section.

6 ANALYSIS OF ZZ CETI CANDIDATES

The two diagrams in Figures 7 and 9 show a clear over-density at the location of the ZZ Ceti stars. This position in the colour-absolute magnitude diagram is so constrained that we may think they could be used as standard candles. There is therefore no doubts about the true variability nature of the largest fraction of candidates proposed by Eyer et al. (2020). Furthermore, since we started this work, there have been several publications on the ZZ Ceti locus (Vincent et al. 2020; Guidry et al. 2021).

6.1 Remarks on ZZ Ceti star's characteristics

Gaia revealed three features on the white dwarf location in the HR diagram (Gaia Collaboration et al. 2018b): (1) sequence A (most populated), (2) another one called B, and (3) a protruding branch, which was predicted by van Horn (1968) more than 50 years ago to be the crystallization sequence of the core of the white dwarf (Tremblay et al. 2019). It has been hypothesized that the origin of these A and B sequences is from the composition of the thin atmosphere, sequence A being composed of hydrogen and B of hydrogen and helium. We remark that with their envelope's chemical composition, ZZ Ceti stars' pulsation is caused by the κ-mechanism (Winget & Kepler 2008). In Figure 11, ZZ Ceti stars are located on the A sequence and not on the B sequence, suggesting that indeed the A sequence has an adequate amount of hydrogen composition.

6.2 ZZ Ceti stars from *Gaia* EDR3

According to our selection illustrated in Figure 9, 343 ZZ Ceti candidates were identified with *Gaia* EDR3 data. They are cross-matched with known ZZ Ceti stars in literature provided by Córsico et al. (2019). As shown in Table 2, among 261 ZZ Ceti stars that are recognized in the literature, 52 (20%) are in our list. Therefore, we have 291 ZZ Ceti candidates from our list. As explained before, we are confident in the variability nature of these objects and thus we choose not to examine their time-series.

7 ANALYSIS OF V777 HERCULIS CANDIDATES

As discussed in Section 4, 103 V777 Herculis candidates were identified with *Gaia* EDR3 measurements. Ten of them (9.7%) are already classified in the literature as V777 Herculis stars (Córsico et al. 2019; Rowan et al. 2019). This list of targets is cross-matched with ZTF DR5 data to retrieve their time series photometry. The cross-match is conducted by manually searching for the object names within a cone of 10 arcsec radius. Every potential match is inspected visually and compared with the target. If multiple objects are found by the query, the object whose g magnitude is the closest to *Gaia* G mag is chosen. If match candidates have similar coordinates, magnitudes, and colors, the target with the highest number of observations is chosen. Figure 12 illustrates the correlation between the magnitudes of the two surveys for both G and RP bands. The graph displays a clear

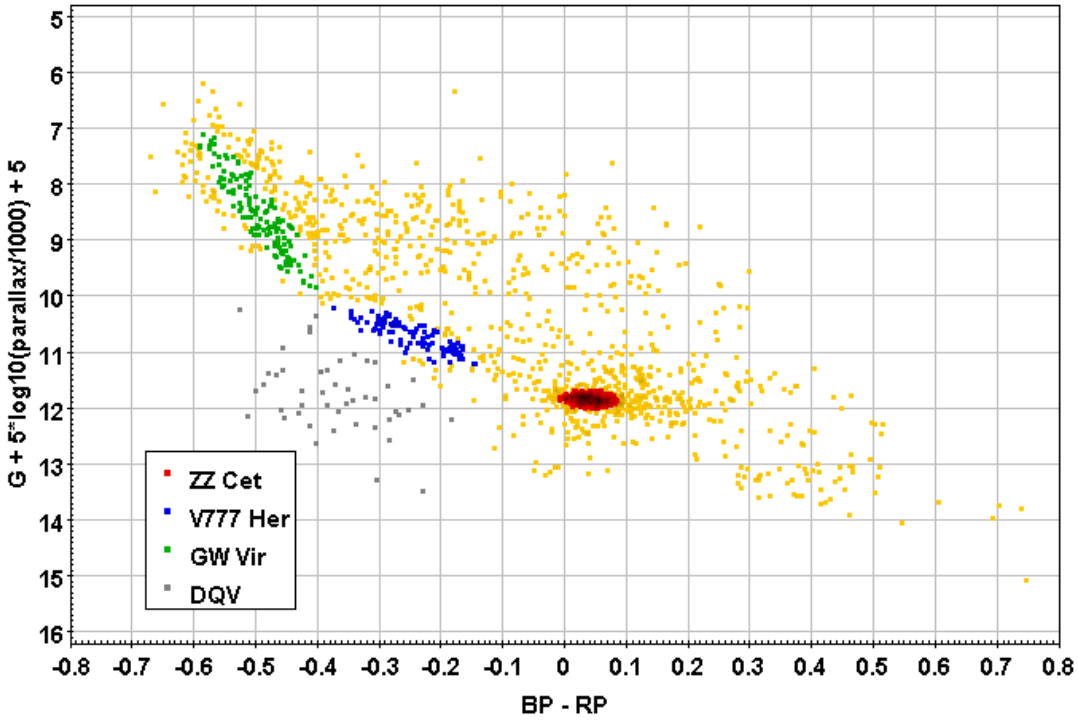

Figure 9. We propose a *Gaia* EDR3 list of ZZ Ceti, V777 Herculis, GW Virginis, and DQV variable white dwarf candidates based on their corresponding over-density regions in the observational HR diagram. The candidates are selected by fitting ellipses over the variability regions. The figure displays the selections among the low-amplitude candidates. There are 343 ZZ Ceti stars, 103 V777 Herculis stars, 132 GW Virginis stars, and 49 DQV stars in this selection.

Table 1. Lomb-Scargle analysis and Chi-square test result of known GW Virginis stars. Even though all stars are variable according to the Chi-square test, the Lomb-Scargle periodogram from ZTF data is not effective in detecting similar pulsating periods as found in the literature.

Name	LS period g (s)	Literature period (s)	Chi-square p-value g	Chi-square p-value r	Variable by Chi-square
NGC1501	561.14	1154 - 5235	8.91e-9	1.24e-33	TRUE
HE1429-1209	927.82	919	9.09e-4	1.29e-18	TRUE
HS2324+3944	7835.9	2005 - 2569	2.13e-18	7.78e-12	TRUE
NGC6852	255.62	1096 - 5128	5.71e-80	0	TRUE
NGC6905	278.79	710 - 912	1.84e-213	4.31e-284	TRUE
NGC7094	577.91	2000 - 5000	1.04e-18	1.19e-14	TRUE
PG0122+200	717.67	336 - 612	1.56e-34	6.21e-17	TRUE
PG1159-035	4900.7	339 - 982	2.51e-17	1.48e-10	TRUE
PG1707+427	447.40	335 - 909	2.08e-188	1.38e-77	TRUE
PG2131+066	630.54	339 - 598	1.12e-12	1.22e-13	TRUE
PNA66-43	289.20	2380 - 6075	5.06e-4	2.89e-35	TRUE
PNJn1	960.16	454	1.60e-2	6.67e-1	FALSE
PNK1-16	454.03	1500 - 1700	1.39e-30	3.13e-37	TRUE
PNVV47	1691.9	261 - 4310	4.66e-03	2.34e-3	FALSE
RX2371-2	907.96	923 - 1825	1.06e-29	9.55e-32	TRUE
RXJ2117.1+3412	43114	694 - 1530	3.00e-08	3.50e-42	TRUE

$N_{\text{literature}}$	$N_{\text{candidates}}$	N_{overlap}
261	343	52

Table 2. The number of confirmed ZZ Ceti stars in literature, of our ZZ Ceti candidates, and the number of stars that appear in both catalogues.

linear relationship and thus confirms the precision of the cross-match selection.

ZTF DR5 data are available in both g and r bands for 64 V777 Herculis candidates. As shown in Figure 13, a Chi-square test on these objects suggests that 28 out of 64 (43.8 %) of them are variable. As this probability is much larger than the type I error probability of 6% (Section 3), it shows that the V777 Herculis region that we select contains a large proportion of variable stars. Among the 64 candidates, we obtain the oscillating frequency in both g and r bands for each star by performing the Lomb-Scargle analysis. As a result, 3 stars shows noticeable periodicity and have similar frequency between g and r data. Their folded light curves are shown in Figure A1 in the appendix, which is available online as supplementary material.

After cross-matching these 3 periodic V777 Herculis candidates

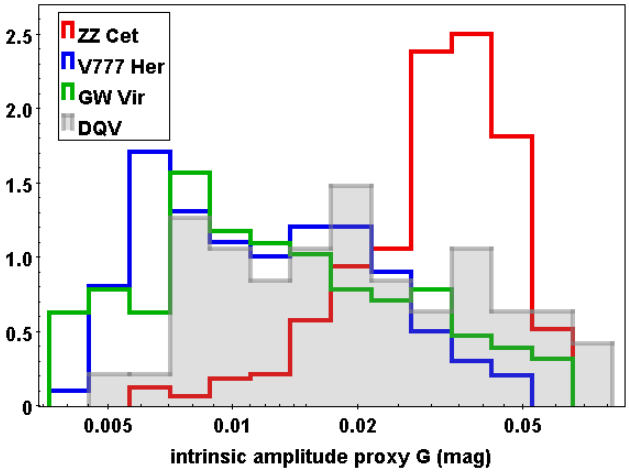

Figure 10. The normalized histogram (unit area) of the *Gaia G* band intrinsic amplitude proxy of the variable white dwarf candidates selection shown in Figure 9. ZZ Ceti stars have the largest amplitudes among the three groups, agreeing with table 2 of Althaus et al. 2010. The amplitude distribution of V777 Herculis stars is skewed towards small amplitudes and has a peak at around -2.2 (around 6 mmag). GW Virginis stars and DQV stars have a relatively broad distribution.

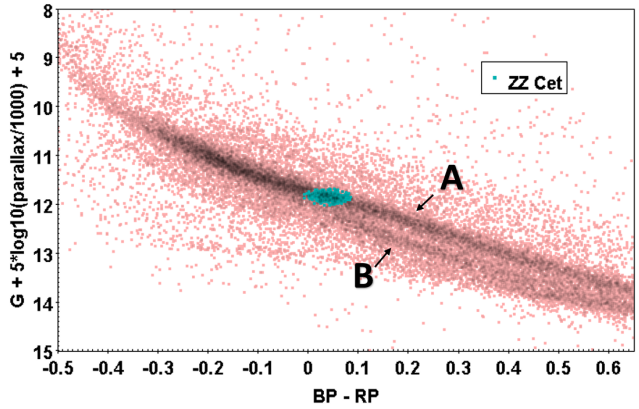

Figure 11. The colour-absolute magnitude diagram shows the two white dwarf sequences A and B. ZZ Ceti candidates are located in the A sequence, as also shown in figure 2 of Vincent et al. 2020.

with literature, Table 3 shows that the star EM UMa (*Gaia* Source ID 1510467090935595008) is already classified as a V777 Herculis pulsating white dwarf. In contrast, the other two candidates are only known as white dwarfs while their periodic behavior is unmentioned. Moreover, the periods of these two stars (6.784 hours and 9.498 hours, as shown in Figure A1 in the online material) and the shapes of their folded light curves are not similar to those of pulsation, but rather binary systems with ellipsoidal variations or spotted stars. Therefore, we remove these two stars from our V777 Herculis candidate list. It can be remarked that Lomb-Scargle analysis helps us not only to detect pulsation but also to clean our lists of pulsating candidates out of binary systems. As 2 out of 64 V777 Herculis candidates that have ZTF DR5 data are discovered to be binaries or spotted stars, we use the similar ratio to estimate the number of binaries and spotted stars in the subset of 39 candidates without ZTF time series (Figure 13). This corresponds to 2 binaries or spotted stars if we take a conservative approach by rounding up the estimation to the nearest integer. On

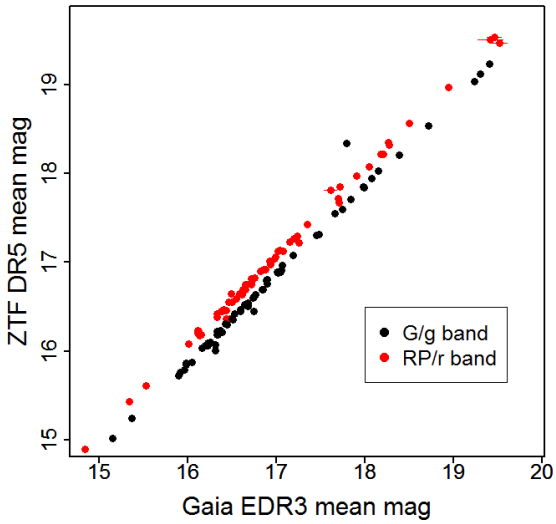

Figure 12. The comparison between *G* and *RP* magnitudes of *Gaia* EDR3 with *g* and *r* magnitudes of ZTF DR5 for 64 V777 Herculis candidates whose ZTF time series are available in both bands. The linear relationship between the two magnitudes emphasizes the consistency of the cross-match.

the other hand, as shown in Section 5, Chi-Square test and Lomb-Scargle analysis are not always sensitive to detect pulsation given the sampling of ZTF. Therefore, the subset of non-variable by Chi-square and non-periodic by Lomb-Scargle can contain true V777 Herculis stars, so we still classify these subsets as candidates. As a result, we estimate that there are 99 V777 Herculis candidates in our selection. However, since we do not know exactly what stars in the unavailable-ZTF-data subset to be binaries or spotted stars, in the summary table of the paper's online version (parts of which can be found in Table 8), we still list all 39 stars as V777 Herculis candidates. They are marked with NA values in the frequency column to infer that we do not have their time series and hence we do not know the origin of their variability.

8 ANALYSIS OF GW VIRGINIS CANDIDATES

Among the 132 GW Virginis candidates in our list, 2 of them were previously classified as a GW Virginis star (Córsico et al. 2019; Althaus et al. 2010; Fontaine & Brassard 2008). Furthermore, applying the same procedure that is discussed in Section 7, we found that 48 out of 80 candidates (60%) with ZTF data in both bands are variable according to the Chi-square test. Hence, compared to our type I error probability, we can infer that there are a large fraction of variable stars in our GW Virginis selection. Among the 80 stars, Lomb-Scargle analysis returns 15 periodic candidates with a similar frequency in *g* and *r* bands. Furthermore, 4 cases only have a significant peak in one band according to the periodogram. For these cases, we run the Lomb-Scargle analysis in both bands with a much narrower frequency range around the examined frequency to check if there is a local peak or if there are aliasing frequencies. As a result, the period peak is also compatible with the other band. Therefore, there are 19 periodic stars among our candidates in the GW Virginis region, and the distribution of their periods is shown in Figure 18.

We perform a cross-match with the literature to check the variability nature of our 19 periodic GW Virginis candidates. As pre-

Table 3. Literature classifications and names of the 3 periodic candidates in the selected V777 Herculis region. Details on the photometric and astronometric measurements of these stars are provided in the online version of the paper (see supporting information) and also from the Centre de Données astronomiques de Strasbourg website (`http://cdsarc.u-strasbg.fr/`). Parts of this table can be found in Table 8.

Gaia EDR3 source_id	Other identifier	Literature Classification	Reference
1510467090935595008	EM UMa	V777 Herculis star	Córsico et al. (2019)
187576000803144704	LAMOST J052026.34+381240.2	White dwarf	Guo et al. (2015)
306181277864983424	–	White dwarf candidate	Gentile Fusillo et al. (2019)

sented in Table 4, among 19 candidates, only PG 1707+427 was already discovered as GW Virginis pulsating white dwarf (Bond et al. 1984). Four stars are classified as binary systems in literature and thus we remove them from our GW Virginis candidate selection, namely PG 0948+534, HS 0727+6003, CRTS J213958.2-074125, and FBS 0125+386. The other 14 candidates are referred to as white dwarfs or white dwarf candidates. In addition, examination of their folded curves (Figure A2 in the online supplementary material) shows that they have a much higher period compared to a common GW Virginis pulsating star: from 5 minutes to 1.7 hours (Córsico et al. 2019). Their periods fall between 3.5 hours to nearly 2 days, which strengthens our hypothesis that they are binary systems with ellipsoidal variations or spotted stars rather than pulsating stars. Therefore, out of 19 periodic candidates in the GW Virginis region, we decide to remove 18 stars from our GW Virginis selection. Using the same calculation described in Section 7, we estimate that there are 12 binaries or spotted stars in the subset of 52 candidates without ZTF data (referred to Figure 13). However, in the summary table of the paper's online version, we mark all these 52 stars as GW Virginis candidates because we do not have enough information to detect their periodicity. As a result, we estimate that there are 102 GW Virginis candidates in our selection. Figure 13 summarizes all the classification steps of the GW Virginis subset.

9 ANALYSIS OF DQV CANDIDATES

For DQV candidates, as illustrated in Figure 13, 60% of the stars that have ZTF data in g and r band are variable according to the Chi-square test (18 out of 30). The percentage of periodic stars from Lomb-Scargle analysis among these 18 variable stars is 56% (10 out of 18 candidates). These stars have similar frequencies in g and r band and have prominent peaks in the power spectrum. Furthermore, in our subset of non-variable stars (according to the Chi-square test), we discover that Gaia EDR3 2529337507976700928 is also periodic. Because the star's amplitude is only around 0.07 mag and the measurement uncertainty is considerable compared to the amplitude, it is reasonable that the Chi-square test is not sensitive enough to detect the star's variability. However, this case is quite subtle to detect the period. While the power spectrum in g band shows a most prominent peak at 34.7 cycles per day with daily aliases, that in r band does not have a highest peak at that frequency. Thus, we rerun the Lomb-Scargle algorithm with the narrower interval of searched frequencies around r band peak (from 30 to 40 cycles per day) and found that there is a local maximum at 37.7 cycles per day in the r band, with multiple aliasing frequencies every 1 cycle per day. Thus, we phase fold both of the light curves with the frequencies of 34.7, 35.7, 36.7, and 37.7 cycles per day. As a result, the frequency of 36.7 cycles per day looks the best visually for both bands, and thus we decide to choose this value as a star's frequency. While this frequency may not be accurate due to the aliasing effect, the periodicity of the star is definite. Hence, we conclude 11 of our DQV candidate selection are periodic and their folded light curves are shown in Figure A3 in the appendix as online material.

Even though the DQV candidates in our list share the same locations in the HR diagram as the known ones in the literature (Córsico et al. 2019), we do not have any known DQVs among our 49 candidates. As shown in Table 5, a cross-match with the literature shows that Gaia EDR3 722446385752579840 is an eclipsing binary (Drake et al. 2014), and thus we eliminate it from our DQV candidate list. Furthermore, Gaia EDR3 2377863773908424448's variability is due to rotation (Liebert et al. 1977), Gaia EDR3 2428675569186550784 is suspected to be rotating although the cause if not fully determined (Lawrie et al. 2013). These two cases agree with the current understanding of DQV's variability. The other 8 stars are either white dwarfs or white dwarf candidates without any mentions of their periodicity in the literature. The periods of these 8 stars are quite homogeneous (Figure 18): 6 of them are below 1 hour, and the other 2 are 3 and 7 hours. Unlike the cases of V777 Herculis and GW Virginis, we do not remove these 8 stars from our selection because it is feasible that rotating stars have frequencies in this range. Therefore, out of 30 stars that have ZTF data in the DQV region, we only notice 1 eclipsing binary. A similar calculation as in Sections 7 and 8 results in an estimation of 47 DQV candidates. All the sub-classifications of DQV candidates can be found in Figure 13.

10 ANALYSIS OF CANDIDATES WHOSE *GAIA* TIME SERIES ARE PUBLIC

10.1 Period search for the 16 candidates

Among 5,387 *Gaia* DR2 variable white dwarf candidates published in Eyer et al. (2020), 16 candidates have publicly available *Gaia* time series data: 12 sources are in the `vari_short_timescale` table, while the other 3 and 1 sources are misclassified as RR Lyrae and δ Scuti stars, respectively. To simplify the notation, the candidates are denoted by a number from 1 to 16. Their corresponding numbers, classifications, and locations on the colour-absolute magnitude diagram can be found in Table 6 and Figure 14. Among them, stars number 1 (RA of 80.41243 degrees and Dec. of 43.99837 degrees) and 7 (RA of 202.7243 degrees and Dec. of 45.13756 degrees), even though they are in the DR2 list of variable white dwarfs candidates, are not in our EDR3 list because their magnitudes are dimmer than our magnitude criterion of 19.5 mags (Section 4). For the other 14 stars, 9 stars have a high amplitude and 5 stars have a low amplitude (as illustrated in Section 4).

The frequency obtained from the Lomb-Scargle periodogram for each band is shown in Table 6. Since ZTF does not cover the whole sky, some candidates will not have ZTF data and thus will be marked with "NA" (not available) in the result table. Out of 16 candidates whose *Gaia* time series are available, 12 candidates display periodicity. Results are summarized in the Venn diagram in Figure 16. In this diagram, the intersection region shows the number of stars whose

Table 4. Literature classifications and names of the 19 periodic candidates in the selected GW Virginis region. The photometric and astronometric information of these stars are provided in the online version of the paper (see supporting information) and also from the Centre de Données astronomiques de Strasbourg website (`http://cdsarc.u-strasbg.fr/`).

Gaia EDR3 source_id	Other identifier	Literature Classification	Reference
1001088333316993536	–	White dwarf candidate	Gentile Fusillo et al. (2019)
1020641700210987520	PG 0948+534	White dwarf, variable of RS CVn type	Drake et al. (2014)
1085903148454238208	HS 0727+6003	DO Hot white dwarf, Eclipsing Binary	Dreizler et al. (1995), Drake et al. (2014)
1355161726346266112	PG 1707+427	GW Virginis star	Bond et al. (1984)
1503131458592587264	PG 1342+444	White dwarf	Tremblay et al. (2011)
1697669356564165632	HS 1517+7403	White dwarf	Heber et al. (1996)
1807309147099442432	–	White dwarf candidate	Gentile Fusillo et al. (2019)
1884773525142393728	–	White dwarf candidate	Gentile Fusillo et al. (2019)
2061416695278519808	–	White dwarf candidate	Gentile Fusillo et al. (2019)
2667317799127474944	CRTS J213958.2-074125	White dwarf candidate, eclipsing binary	Gentile Fusillo et al. (2019),Drake et al. (2014)
323342459647016448	FBS 0125+386	White dwarf, cataclysmic variable	Girven et al. (2011),Downes et al. (2001)
3370796406708211200	–	White dwarf candidate	Gentile Fusillo et al. (2019)
3759364193922337152	PG 1106-085	White dwarf candidate, hot subdwarf	Gentile Fusillo et al. (2019),Geier et al. (2017)
3842377248804727168	SDSS J091748.20+001041.6	White dwarf candidate	Gentile Fusillo et al. (2019)
4453903355360209152	PG 1612+112	White dwarf	Kleinman et al. (2013)
4587412856136181376	–	White dwarf candidate	Gentile Fusillo et al. (2019)
6609580078678720512	Ton S 77	White dwarf candidate	Gentile Fusillo et al. (2019)
921460739159662080	KUV 08026+4118	White dwarf	Limoges & Bergeron (2010)
953685015492787456	–	White dwarf candidate	Gentile Fusillo et al. (2019)

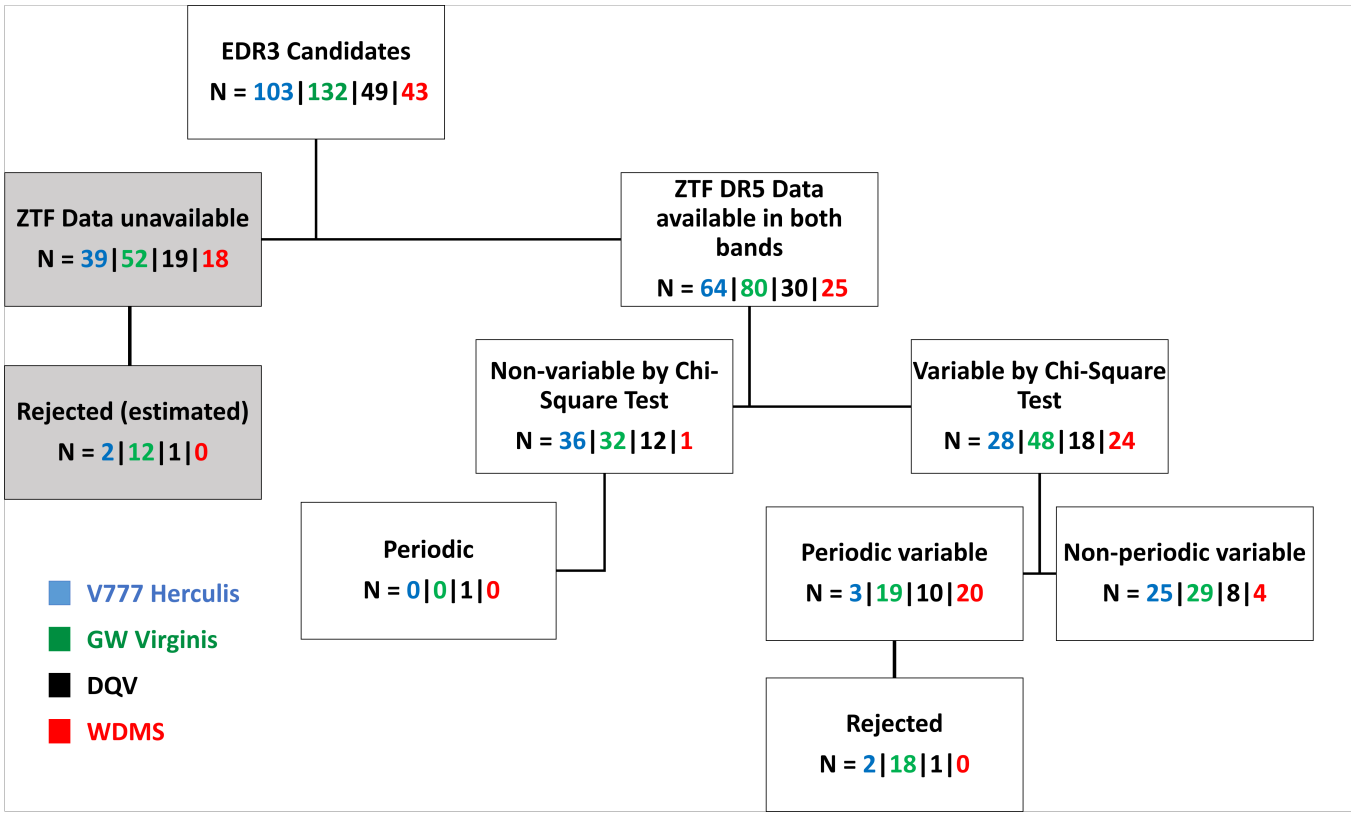

Figure 13. This hierarchy chart summarizes the categories of V777 Herculis (blue), GW Virginis (green), DQV (black), and WDMS (red) candidates using ZTF data. The gray boxes are candidates whose data is not adequate to provide reliable variability classifications in the scope of this study.

period is the same between the two independent surveys. Specifically, targets numbers 5, 6, 8, and 11 have a similar period in *Gaia* and ZTF. Eight stars (numbers 2, 3, 4, 9, 13, 14, 15, and 16) show periodic behaviour in only one survey data. The other 4 stars in the list (1, 7, 10, and 12) do not exhibit any periodicity in both surveys' time series. To sum up, among 12 periodic candidates, 5 stars are detected by ZTF only, 3 stars by *Gaia* data only, and 4 stars by both ZTF and *Gaia*. The folded light curves of these stars are provided in Figures A4 and A5 of the online supplementary appendix.

After examining the phase curves of the periodic candidates, we

Table 5. Literature classifications and names of the 11 periodic candidates in the selected DQV region. The photometric and astronometric measurements of these stars will be provided in the online version of the paper (see supporting information) and also from the Centre de Données astronomiques de Strasbourg website (http://cdsarc.u-strasbg.fr/).

Gaia ED3 source_id	Other identifier	Literature Classification	Reference
1891820737544168576	–	White dwarf candidate	Gentile Fusillo et al. (2019)
2082008971824158720	–	White dwarf candidate	Gentile Fusillo et al. (2019)
2116343627572365440	–	White dwarf candidate	Gentile Fusillo et al. (2019)
2377863773908424448	Feige 7	Rotating magnetic white dwarf	Liebert et al. (1977)
2428675569186550784	PHL 657	Periodic DQ magnetic white dwarf	Lawrie et al. (2013)
2529337507976700928	SDSS J005045.81-032655.6	White dwarf candidate	Gentile Fusillo et al. (2019)
2533306985471073920	PB 6365	White dwarf candidate	Gentile Fusillo et al. (2019)
2861452348130844160	SDSS J000637.93+310415.7	White dwarf candidate	Gentile Fusillo et al. (2019)
722446385752579840	Ton 527	White dwarf, eclipsing binary	Drake et al. (2014)
861044048386465664	SBSS 1107+603	White dwarf	Kleinman et al. (2013)
898348313253395968	SDSS J071816.41+373139.1	White dwarf candidate	Gentile Fusillo et al. (2019)

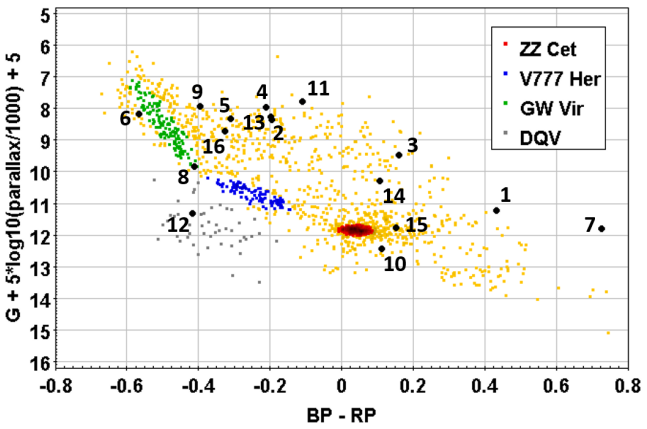

Figure 14. The colour-absolute magnitude diagram shows the locations of 16 variable white dwarf candidates whose *Gaia* time series are available. The candidates are numbered similarly as in Table 6. Four regions of variable white dwarfs ZZ Ceti, V777 Herculis, GW Virginis, and DQV described in Figure 8 are represented by the colour red, blue, green, and grey, respectively.

notice a peculiar characteristic that 6 candidates (numbers 2, 4, 5, 9, 11, 16) have larger amplitude in the red band than in the blue band (folded light curves shown in Figure 15). On the colour-absolute magnitude diagram in Figure 14, these 6 candidates are all located in a region that we suspect to host binary systems. Hence, we hypothesize that this difference in the amplitude across colour originates from the ellipsoidal variation of a binary between a white dwarf and a main sequence star. When the blue flux of the white dwarf is large enough to outweigh the blue flux of the whole system, the relative change of flux in the blue band will be much less than that in the red band during the maximum and the minimum of the variation. It is important to assert that this behavior does not happen to all binaries involving a white dwarf, but to a specific combination of the two components in which the blue flux of the white dwarf dominates that of the main sequence star. This specificity is also reflected in the clumped region in Figure 14 (between 8 to 9 absolute magnitude and between -0.4 to -0.1 colour index). Therefore, we use this characteristic as a conservative criterion to detect white dwarf-main sequence (WDMS) binaries, which will be discussed in Section 11.

10.2 Comparison with classifications in literature

The classifications of the 12 periodic variable stars shown in Table 6 were checked with the literature and presented in Table 7. Candidate numbers 3, 4, 5, 9, and 15 were found to be binary star systems, for which we can confirm the periodic variability. As the other 7 candidates are not classified as variable stars in literature, our analysis detects them as new periodic variables.

11 ANALYSIS OF WDMS CANDPPENDIIDATES

As discussed in Section 10, through ellipsoidal modulation, WDMS systems with a highly blue white dwarf component can produce a larger amplitude in the red band than in the blue band. Thus, we propose a method to detect these systems, by assuming that the standard deviation in the *RP*-band ($\sigma_{\rm RP}$) will be larger than that in the *BP*-band ($\sigma_{\rm BP}$), where

$$\sigma_{\rm RP} = \frac{1.086\ \sqrt{\texttt{phot\_rp\_n\_obs}}}{\texttt{phot\_rp\_mean\_flux\_over\_error}}$$
$$\sigma_{\rm BP} = \frac{1.086\ \sqrt{\texttt{phot\_bp\_n\_obs}}}{\texttt{phot\_bp\_mean\_flux\_over\_error}}. \quad (12)$$

Regarding the limit of the criterion, we take a conservative approach by selecting the minimum $\sigma_{\rm RP}/\sigma_{\rm BP}$ value among the 6 candidates in Figure 15. Therefore, we decide to set a lower limit of such ratio to 1.9. Furthermore, since ellipsoidal modulation often has large photometric variation, we apply this criterion on the high amplitude candidates (referred to Section 4) to select 43 WDMS candidates. The result of this selection is displayed in Figure 17. According to the diagram, the concentration of our WDMS candidates in the binary sequence is consistent with that in Figure 14.

Figure 13 displays the result of Lomb-Scargle analysis and Chi-square test for our 43 WDMS candidates: 96% (24 over 25) of the candidates are variable and 80% (20 over 25) are periodic with similar frequencies between two bands. These high percentages emphasize the efficiency of our method to detect periodic light curves. The folded light curves of the periodic stars are shown in Figure A6 (provided in the online material), and all of them have amplitude in ZTF *g* band larger than in *r* band. Also, Figure 18 display the histogram of the periods of our periodic WDMS candidates. A large fraction of these periods lies between 1 and 10 hours, which is reasonable for a period of binary systems.

In addition, the Lomb-Scargle analysis of the other high amplitude candidates that do not satisfy our requirement of the $\sigma_{\rm RP}/\sigma_{\rm BP}$ ratio

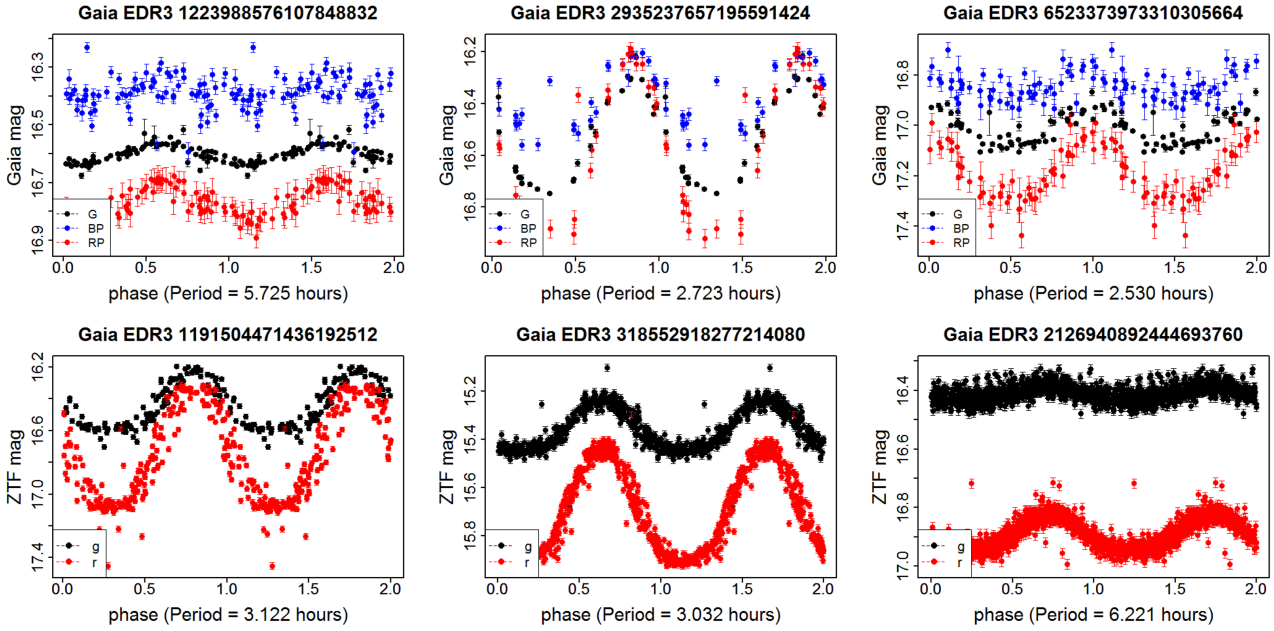

Figure 15. Six candidates whose amplitude is larger in red band than blue band among 16 candidates that have *Gaia* time series.

Table 6. The table displays the Lomb-Scargle analysis results of the 16 candidates whose *Gaia* time series are available. The periods were computed for each candidate of each survey independently. The classification from previous sections is listed in the third column. Two candidates do not have classifications (denoted as NA) because their mean *G* magnitudes exceed our criterion limit. The values in bold indicate that the candidates demonstrate clear periodic variability with that period. The candidates with source_id followed by an asterisk have amplitude in *RP* larger than *BP*. Details on the photometric and astronometric measurements of these stars will be provided in the online version of the paper (see supporting information) and also from the Centre de Données astronomiques de Strasbourg website (`http://cdsarc.u-strasbg.fr/`).

Gaia EDR3 source_id	Number	Classification	*Gaia G*	*Gaia RP*	*Gaia BP*	*ZTF g*	*ZTF r*
207617138541901312	1	NA	4.57 mins	2.89 mins	10.09 mins	23.96 hrs	23.97 hrs
318552918277214080*	2	high amplitude	11.31 mins	11.31 mins	11.31 mins	**3.03 hrs**	**3.03 hrs**
849625139095603072	3	high amplitude	1.57 mins	2.42 mins	2.30 mins	**1.91 hrs**	**1.91 hrs**
1191504471436192512*	4	high amplitude	9.23 mins	6.43 mins	4.50 mins	**3.12 hrs**	**3.12 hrs**
1223988576107848832*	5	low amplitude	**5.73 hrs**	**5.73 hrs**	1.81 mins	1.49 mins	**5.73 hrs**
1286055427676135808	6	low amplitude	**23.27 hrs**	1.44 hrs	51.42 mins	**23.27 hrs**	**23.28 hrs**
1550043320485422208	7	NA	1.72 mins	5.72 mins	2.31 mins	2.05 mins	2.22 mins
2061416695278519808	8	low amplitude	**5.32 hrs**	3.60 mins	6.88 mins	**5.32 hrs**	**5.31 hrs**
2126940892444693760*	9	low amplitude	3.59 mins	2.30 mins	1.53 mins	**6.22 hrs**	**6.22 hrs**
2930889294867085440	10	high amplitude	2.48 mins	1.70 mins	1.47 mins	14.06 mins	2.00 days
2935237657195591424*	11	high amplitude	**2.72 hrs**	**2.72 hrs**	1.45 mins	**2.72 hrs**	**2.72 hrs**
3302538209462061696	12	high amplitude	2.51 mins	3.71 mins	5.37 mins	29.13 mins	NA
3471231910527986432	13	high amplitude	1.89 mins	9.23 mins	**14.39 mins**	NA	NA
4318508939464901760	14	high amplitude	1.57 mins	3.33 mins	26.11 mins	**1.56 hrs**	**1.56 hrs**
5645504991845223936	15	high amplitude	**16.12 hrs**	**16.12 hrs**	3.04 mins	NA	NA
6523373973310305664*	16	low amplitude	**2.53 hrs**	**2.53 hrs**	1.74 mins	NA	NA

reveals that 27% of them are periodic. The periods and amplitudes of these stars are also included in the online version of the paper. Even though these periodic stars may contain WDMS systems, we do not classify them as such since they can also be white dwarf-white dwarf binary or spotted stars. It is difficult to differentiate those types from each other just from photometric measurements, while we want to take a more precise approach to select WDMS systems.

To evaluate the significance of the obtained percentages, we employ stratified random sampling to select white dwarfs from Gentile Fusillo et al. (2019)'s catalogue. Since the distribution of the candidates' *G* magnitude from Gentile Fusillo et al. (2019) is not uniform, we divided the range from 13.5 to 19.5 mags into 800 small bins and select 1 star from each bin. This ensures that our sample is uniformly distributed and thus contains representatives at all magnitudes. Since some bins do not have targets, as a result, we select 776 targets, and 483 of them have ZTF data. According to Lomb-Scargle, only 10 of them are periodic. Conversion from the sample percentage to population percentage gives an estimation of below 1%. Compared to the value of 80% that we get in our WDMS selection, this emphasizes the efficiency of our method to detect periodic light curves.

Table 7. Classifications and names from literature for 12 periodic variable stars among 16 white dwarfs candidates with *Gaia* time series. The targets whose source_id is followed by an asterisk have the amplitude in *RP* band larger than in *BP* band.

Gaia EDR3 source_id	Number	Name	Literature Classification	Reference
3185529182772140 80*	2	FBS 0145+363	Hot subdwarf candidate	Geier et al. (2017)
849625139095603072	3	EK UMa	Cataclysmic variable	Gentile Fusillo et al. (2019)
1191504471436192512*	4	NN Ser	Nova, Eclipsing binary	Samus' et al. (2003), Drake et al. (2014)
1223988576107848832*	5	Ton 243	White dwarf-Main sequence binary	Rebassa-Mansergas et al. (2010)
1286055427676135808	6	CBS 389	DA White dwarf	Girven et al. (2011)
2061416695278519808	8	–	White dwarf candidate	Gentile Fusillo et al. (2019)
2126940892444693760*	9	KIC 8490027	Catalysmic variable	Howell et al. (2013)
2935237657195591424*	11	–	White dwarf candidate	Gentile Fusillo et al. (2019)
3471231910527986432	13	EC 12250-3026	Hot subdwarf	Kilkenny et al. (1997)
4318508939464901760	14	2MASS J19412506+1522553	High proper-motion star	Gaia Collaboration (2018)
5645504991845223936	15	RX J0838.7-2827	Cataclysmic Variable	Halpern et al. (2017)
6523373973310305664*	16	–	White dwarf candidate	Gentile Fusillo et al. (2019)

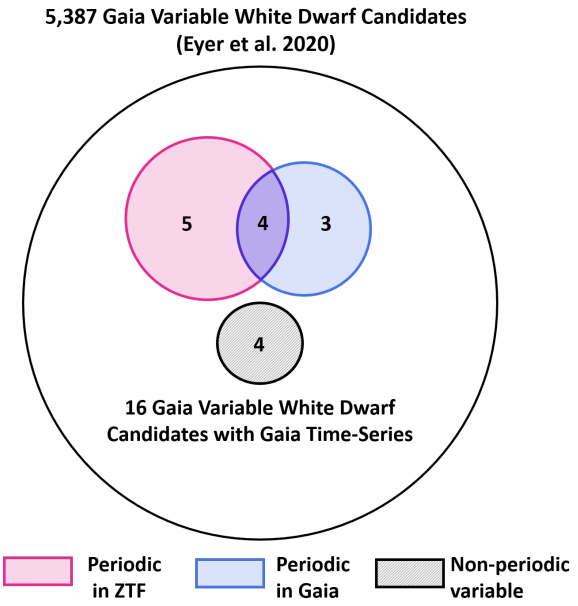

Figure 16. The Venn Diagram summarizes the analysis result of 16 candidates that have *Gaia* time series. Among them, 12 cases show periodicity in their light curves. The intersection shows the cases in which there is a similar period independently found between *Gaia* and ZTF. There are 4 candidates in this intersection region.

12 CROSS-MATCH WITH KNOWN CATACLYSMIC VARIABLES AND KNOWN WDMS BINARIES

A cross-match with Pala et al. (2020)'s catalogue of cataclysmic variables (CVs) within 150 pc results in 12 targets in our set of variable candidates. Among them, 3 stars have a high amplitude, meaning that the intrinsic amplitude proxy in g band is larger or equal to 0.07 mag, and 9 stars have low amplitudes. The locations of these stars in the colour-absolute magnitude diagram are displayed in Figure 19. All CVs have absolute luminosities around 11–12 mag. Moreover, they are redder than the ZZ Ceti clump, forming a horizontal region in the diagram.

Similarly, we conduct a cross-match with the catalogue of Rebassa-Mansergas et al. (2010) to evaluate the effectiveness of our criterion in detecting WDMS binaries. The WDMS binaries in the catalogue are defined by their SDSS spectroscopy data, thus the selection procedure is independent of ours. Only one of our binary candidates is in common with their WDMS binaries. In fact, this low number is not a surprise as our WDMS selection is limited to high amplitude and ellipsoidal variation with a specific combination, while Rebassa-Mansergas et al. (2010)'s selection covers more general WDMS cases.

13 DISCUSION AND CONCLUSION

By evaluating the catalogue of *Gaia* DR2 pulsating white dwarfs (Eyer et al. 2020) with the revised photometric and astrometric measurements of EDR3, we refine the existing classifications of variable white dwarfs. We employ the Lomb-Scargle analysis as well as the Chi-square test with the ZTF DR5 time series to detect their frequency and variability. The partial list of all our 1743 variable candidates along with their periodicity, classifications, frequencies, and amplitudes are provided in Table 8. In the table, *NA* values suggest that ZTF data is not available for those stars or we do not use ZTF data for the analysis. The full list of our candidates will be provided in the online version of the paper and from the Centre de Données astronomiques de Strasbourg website (`http://cdsarc.u-strasbg.fr/`).

The Lomb-Scargle analysis also helps us refine our candidate by detecting suspected binary systems or spotted stars. Among 3 periodic stars found in the V777 Herculis region, 2 are potential binaries and spotted stars. The ratios are 18 out of 19 periodic stars and 1 out of 11 periodic stars for GW Virginis and DQV region, respectively. After removing those suspected binaries and spotted stars, with EDR3 data, we propose 343 ZZ Ceti candidates, and estimate that there are 99, 102, and 47 candidates for V777 Herculis, GW Virginis, and DQV types, respectively. Furthermore, we derive a criterion on the standard deviations of *RP* and *BP* band to detect 43 candidates of WDMS binaries.

For all types of candidates discussed in this paper, the periods from Lomb-Scargle analysis are between 6.5 minutes and 2.1 days and their ZTF g amplitudes are between 0.06 and 0.4 mag. Even though we do not have a large fraction of periodic V777 Herculis and GW Virginis stars from Lomb-Scargle, we obtain a high percentage of variability: 42% for V777 Herculis candidates and 48% for GW Virginis candidates. As shown in Section 5, Chi-square test and Lomb-Scargle analysis are not the most effective method to study the pulsating white dwarfs, given their small amplitudes, the complexity of the signals, the sampling, and the precision of *Gaia* and

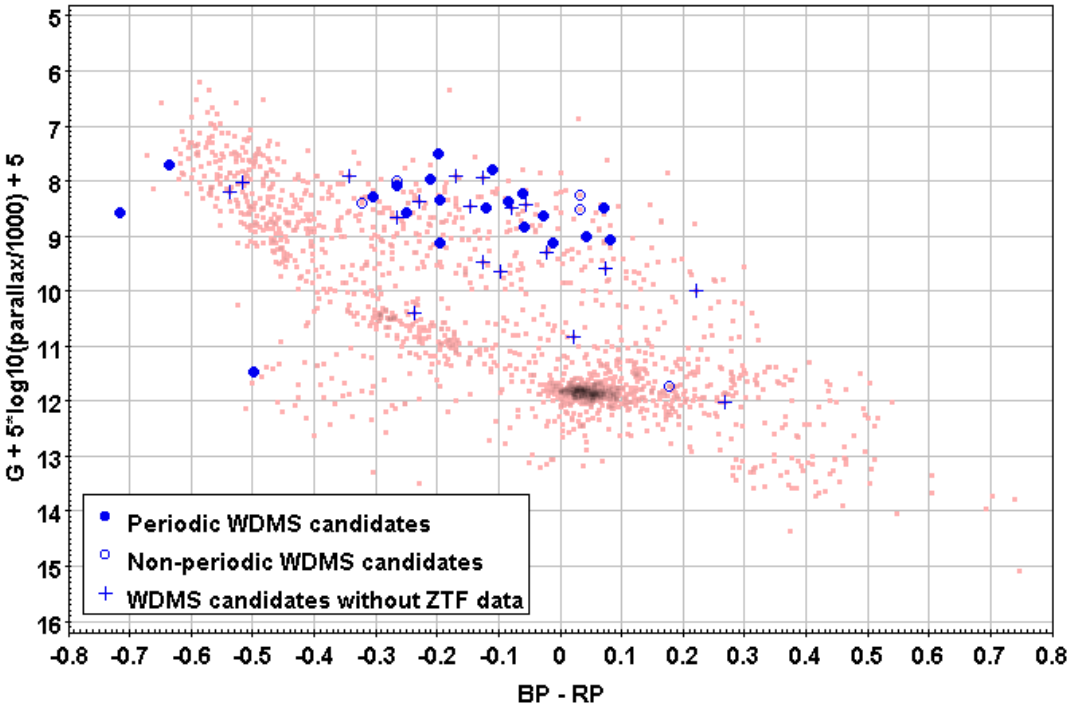

Figure 17. The colour-absolute magnitude diagram displays our WDMS binary candidates. We select potential WDMS systems by setting a lower limit of 1.9 for the ratio between standard deviation in the *RP* and *BP* bands. In the diagram, an over-density can be noticed on the red side of the GW Virginis instability strip. According to this selection, there are 43 WDMS binaries candidates, and their Lomb-Scargle analysis results are also reflected in the diagram. It should be noted that this selection is conservative to specific WDMS systems whose blue flux of the white dwarf accounts mainly for the blue flux of the whole system.

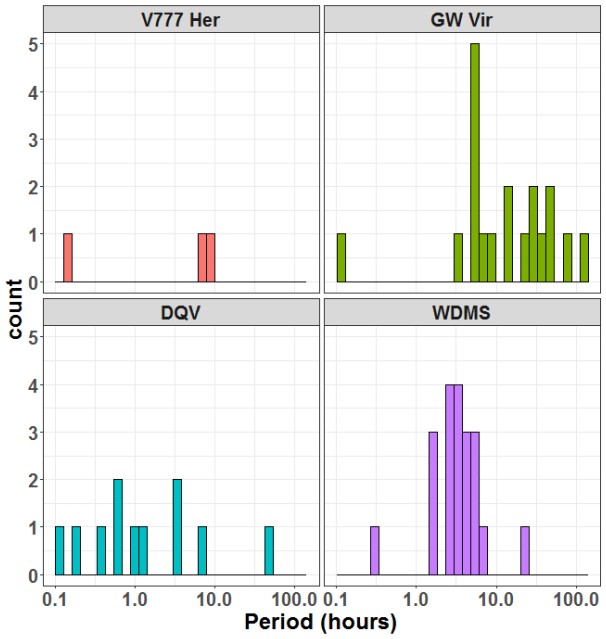

Figure 18. The histograms shows the period distribution of the periodic candidates from different regions in the study. Most of the periods of WDMS candidates are concentrated between 1 hour and 10 hours, agreeing with the common periods of binary systems. However, we also detect periodic stars falling in this period range for the cases of V777 Herculis and GW Virginis candidates. Thus, we believe those candidates are binary stars or spotted stars, rather than pulsating stars.

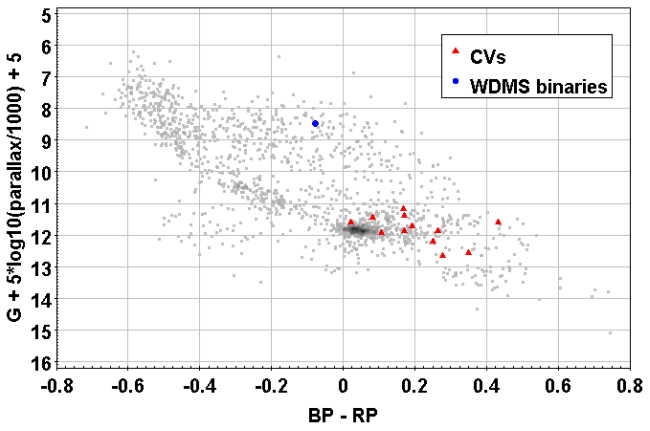

Figure 19. The colour-absolute magnitude diagram showing the positions of 12 known cataclysmic variables (CVs) and 1 WDMS binary in our list of variable candidates (Figure 6). The cross-match was conducted with the cataclysmic variable list of Pala et al. 2020 and the WDMS binary list of Rebassa-Mansergas et al. 2010.

ZTF. However, those percentages are significant if we compare them to a random sample of white dwarfs. Specifically, the variability percentage of a stable white dwarf region is 6%.

For DQV candidates, we obtain 34% of periodic stars and 59% of variable stars. For WDMS candidates, those results are 80% and 96%. The periodicity percentage of a random sample of white dwarfs is below 1%, thus affirming the effectiveness of our selection criteria, even if their non-optimal efficiency makes them conservative.

In our analysis of the 16 variable white dwarfs whose *Gaia* time

series are available, we identify 7 periodic stars using *Gaia* data and 9 periodic stars using ZTF data. Among them, 4 stars whose source ids are 1223988576107848832, 1286055427676135808, 2061416695278519808, and 2935237657195591424, share consistent frequencies regardless of being studied with two independent data sets. Thus, there is more confidence in determining their oscillating periods.

With more time series data being published in *Gaia* DR3 (i.e., 10 to 13 million sources detected as variable), we will have more possibilities to explore the *Gaia* time series and understand the origin of their high standard deviation in EDR3 data (the criterion we used in this article). In *Gaia* DR3, a list of variable white dwarfs will also be published, and thus it will be interesting to compare that list with our list. Moreover, the potential of detecting variable white dwarfs thanks to *Gaia* and ZTF is large. Efforts should be made so that the *Gaia* DPAC can use these discoveries for *Gaia* DR4 in the supervised classification with revised training sets.

ACKNOWLEDGEMENTS

We thank Richard I. Anderson, Anthony Brown, Boris Gaensicke, and Nami Mowlavi for discussions and comments. We also thank the ThinkSwiss Research Scholarship for financially support Thinh Nguyen to do research at the University of Geneva. This work has made use of data from the European Space Agency (ESA) mission *Gaia* (https://www.cosmos.esa.int/gaia), processed by the *Gaia* Data Processing and Analysis Consortium (DPAC, https://www.cosmos.esa.int/web/gaia/dpac/consortium). Funding for the DPAC has been provided by national institutions, in particular the institutions participating in the Gaia Multilateral Agreement.

DATA AVAILABILITY

The data underlying this article are available in the public *Gaia* archive (https://gea.esac.esa.int/archive/) and the public ZTF archive (https://irsa.ipac.caltech.edu/Missions/ztf.html).

REFERENCES

Althaus L. G., Córsico A. H., Isern J., García-Berro E., 2010, A&ARv, 18, 471
Becker R. A., Chambers J. M., Wilks A. R., 1988, The new S language. Chapman & Hall
Bellm E. C., et al., 2019, PASP, 131, 018002
Belokurov V., Erkal D., Deason A. J., Koposov S. E., De Angeli F., Evans D. W., Fraternali F., Mackey D., 2017, MNRAS, 466, 4711
Bond H. E., Grauer A. D., Green R. F., Liebert J. W., 1984, ApJ, 279, 751
Brinkworth C. S., Marsh T. R., Morales-Rueda L., Maxted P. F. L., Burleigh M. R., Good S. A., 2005, MNRAS, 357, 333
Córsico A. H., Althaus L. G., Miller Bertolami M. M., Kepler S. O., 2019, A&ARv, 27, 7
Cuypers J., 2012, Technical Report GAIA-C7-SP-ROB-JCU-002-4, Period Search - Software Requirement Specification. Royal Observatory of Belgium
Downes R. A., Webbink R. F., Shara M. M., Ritter H., Kolb U., Duerbeck H. W., 2001, PASP, 113, 764
Drake A. J., et al., 2014, ApJS, 213, 9
Dreizler S., Heber U., Napiwotzki R., Hagen H. J., 1995, A&A, 303, L53
Evans D. W., et al., 2018, A&A, 616, A4
Eyer L., 1998, PhD thesis, University of Geneva, doi:10.13097/archive-ouverte/unige:141153
Eyer L., et al., 2020, in Neiner C., Weiss W. W., Baade D., Griffin R. E., Lovekin C. C., Moffat A. F. J., eds, Stars and their Variability Observed from Space. pp 11–17 (arXiv:1912.07659)
Fontaine G., Brassard P., 2008, PASP, 120, 1043
Gaia Collaboration 2018, VizieR Online Data Catalog, p. I/345
Gaia Collaboration et al., 2016a, A&A, 595, A1
Gaia Collaboration et al., 2016b, A&A, 595, A2
Gaia Collaboration et al., 2018a, A&A, 616, A1
Gaia Collaboration et al., 2018b, A&A, 616, A10
Gaia Collaboration et al., 2019, A&A, 623, A110
Gaia Collaboration et al., 2021, A&A, 649, A1
Geier S., Østensen R. H., Nemeth P., Gentile Fusillo N. P., Gänsicke B. T., Telting J. H., Green E. M., Schaffenroth J., 2017, A&A, 600, A50
Gentile Fusillo N. P., et al., 2019, MNRAS, 482, 4570
Girven J., Gänsicke B. T., Steeghs D., Koester D., 2011, MNRAS, 417, 1210
Guidry J. A., et al., 2021, ApJ, 912, 125
Guo J., Zhao J., Tziamtzis A., Liu J., Li L., Zhang Y., Hou Y., Wang Y., 2015, MNRAS, 454, 2787
Halpern J. P., Bogdanov S., Thorstensen J. R., 2017, ApJ, 838, 124
Heber U., Dreizler S., Hagen H. J., 1996, A&A, 311, L17
Holl B., et al., 2018, A&A, 618, A30
Howell S. B., et al., 2013, AJ, 145, 109
Kilkenny D., O'Donoghue D., Koen C., Stobie R. S., Chen A., 1997, MNRAS, 287, 867
Kleinman S. J., et al., 2013, ApJS, 204, 5
Lawrie K. A., Burleigh M. R., Dufour P., Hodgkin S. T., 2013, MNRAS, 433, 1599
Liebert J., Angel J. R. P., Stockman H. S., Spinrad H., Beaver E. A., 1977, ApJ, 214, 457
Limoges M. M., Bergeron P., 2010, ApJ, 714, 1037
Lindegren L., et al., 2018, A&A, 616, A2
Lindegren L., et al., 2020, arXiv e-prints, p. arXiv:2012.03380
Lomb N. R., 1976, Ap&SS, 39, 447
Macfarlane S. A., et al., 2017, MNRAS, 470, 732
Mignard F., et al., 2008, in Jin W. J., Platais I., Perryman M. A. C., eds, IAU Symposium Vol. 248, A Giant Step: from Milli- to Micro-arcsecond Astrometry. pp 224–230 (arXiv:0712.0889), doi:10.1017/S1743921308019145
Mowlavi N., et al., 2021, A&A, 648, A44
Pala A. F., et al., 2020, MNRAS, 494, 3799
Percy J. R., 2011, Understanding Variable Stars. Cambridge University Press
Rebassa-Mansergas A., Gänsicke B. T., Schreiber M. R., Koester D., Rodríguez-Gil P., 2010, MNRAS, 402, 620
Riello M., et al., 2020, arXiv e-prints, p. arXiv:2012.01916
Rowan D. M., Tucker M. A., Shappee B. J., Hermes J. J., 2019, MNRAS, 486, 4574
Ruf T., 1999, Biological Rhythm Research, 30, 178
Samus' N. N., et al., 2003, Astronomy Letters, 29, 468
Scargle J. D., 1982, ApJ, 263, 835
Tremblay P. E., Bergeron P., Gianninas A., 2011, ApJ, 730, 128
Tremblay P. E., Fontaine G., Freytag B., Steiner O., Ludwig H. G., Steffen M., Wedemeyer S., Brassard P., 2015, ApJ, 812, 19
Tremblay P.-E., et al., 2019, Nature, 565, 202
Vincent O., Bergeron P., Lafrenière D., 2020, AJ, 160, 252
Williams K. A., Montgomery M. H., Winget D. E., Falcon R. E., Bierwagen M., 2016, ApJ, 817, 27
Winget D. E., Kepler S. O., 2008, ARA&A, 46, 157
Winget D. E., et al., 1991, ApJ, 378, 326
van Horn H. M., 1968, ApJ, 151, 227

APPENDIX A: FOLDED LIGHT CURVES (ONLINE MATERIAL)

This paper has been typeset from a TEX/LATEX file prepared by the author.

Table 8. Selected rows from the table summarizing the analyzing result of our 1743 variable white dwarf candidates. In the table, *NA* infers that we do not have or do not obtain ZTF data for the analysis.

dr2_source_id	edr3_source_id	ra (deg)	dec (deg)	parallax (mas)	parallax_error (mas)	pm (mas/yr)	pmra (mas/yr)	pmdec (mas/yr)
(1)	(2)	(3)	(4)	(5)	(6)	(7)	(8)	(9)
761769968148078208	761769968148078208	166.9658	35.07929	3.890586	0.240606	75.4202	-73.7082	15.97829
4322122179510423296	4322122179512445568	292.9217	16.80738	7.907328	0.047735	30.65457	19.83774	23.37021
2667317799127474944	2667317799127474944	324.993	-7.69073	1.933636	0.088499	33.95377	17.80679	-28.9098
5758736375755925760	5758736375755925760	138.7966	-4.95856	2.263913	0.066419	13.60487	-9.96517	-9.26217
2533306985471073920	2533306985471073920	19.54309	-1.93677	9.983024	0.078762	27.04923	25.39837	-9.30503
4058112910664256384	4058112910664256384	260.3424	-31.5288	6.770454	0.067803	31.63642	0.671154	-31.6293
2126940892444693760	2126940892444693760	289.8795	44.54546	1.866686	0.042364	17.17731	-10.3964	-13.6739
1772627698499060096	1772627698499060096	326.6877	16.18621	0.914708	0.299551	8.2271	-5.95029	-5.68148
3909559715659399808	3909559715659399808	174.6112	6.322027	4.791853	0.215601	60.841	-58.8836	-15.3084
5362131777018335360	5362131777028219904	166.1606	-49.0361	2.999679	0.235039	19.25338	-0.76875	-19.238

phot_g_mean_mag (mag) (10)	phot_g_mean_mag_err (mag) (11)	phot_bp_mean_mag (mag) (12)	phot_bp_mean_mag_err (mag) (13)	phot_rp_mean_mag (mag) (14)	phot_rp_mean_mag_err (mag) (15)
18.83558	0.004765	18.84088	0.058316	18.81228	0.064812
15.91232	0.001003	15.79489	0.003093	16.13468	0.004298
16.66344	0.002796	16.49362	0.010669	17.00802	0.008452
16.39003	0.001267	16.21408	0.005510	16.75057	0.005550
16.68631	0.001340	16.50901	0.007430	17.00898	0.010641
16.41636	0.001381	16.28307	0.003238	16.6946	0.004514
16.56669	0.002206	16.42598	0.004760	16.82221	0.013767
19.31121	0.005379	19.2257	0.037614	19.42172	0.084582
18.53621	0.006756	18.62673	0.045379	18.39541	0.038144
19.16556	0.000425	19.34833	0.020794	18.98223	0.027080

classification (16)	frequency (cycles/day) (17)	amplitude_g (mag) (18)	amplitude_r (mag) (19)
ZZ Cet	NA	NA	NA
V777 Her	non periodic	non periodic	non periodic
Low amplitude (rejected GW Vir)	4.83909	0.17385	0.15144
GW Vir	non periodic	non periodic	non periodic
DQV	26.3314	0.06704	0.09233
DQV	NA	NA	NA
Low amplitude	NA	NA	NA
WDMS	4.7645	0.23909	0.3671
High amplitude	non periodic	non periodic	non periodic
High amplitude	NA	NA	NA